
Accelerating Generalized Linear Models by Trading off Computation for Uncertainty

Lukas Tatzel¹ Jonathan Wenger² Frank Schneider¹ Philipp Hennig¹

Abstract

Bayesian Generalized Linear Models (GLMs) define a flexible probabilistic framework to model categorical, ordinal and continuous data, and are widely used in practice. However, exact inference in GLMs is prohibitively expensive for large datasets, thus requiring approximations in practice. The resulting approximation error adversely impacts the reliability of the model and is not accounted for in the uncertainty of the prediction. In this work, we introduce a family of iterative methods that explicitly model this error. They are uniquely suited to parallel modern computing hardware, efficiently recycle computations, and compress information to reduce both the time and memory requirements for GLMs. As we demonstrate on a realistically large classification problem, our method significantly accelerates training compared to competitive baselines by trading off reduced computation for increased uncertainty.

1. Introduction

Generalized Linear Models (GLMs) (Nelder & Wedderburn, 1972) form a fundamental interpretable model class widely used throughout the natural and social sciences. For example, GLMs are applied to count data in biomedicine, categorical data in object classification tasks, or continuous data in time series regression. A GLM assumes the data is generated from an exponential family likelihood, which depends on a latent function mapped through an inverse link function. In a Bayesian treatment of GLMs, a Gaussian linear model (Dobson & Barnett, 2018), or more generally a Gaussian process (GP), is used to model the latent function. Such a probabilistic approach is essential in domains where critical decisions must be made based on limited information, such as in public policy, medicine or robotics.

¹University of Tübingen, Tübingen AI Center ²Columbia University. Correspondence to: Lukas Tatzel <lukas.tatzel@uni-tuebingen.de>, Jonathan Wenger <jw4246@columbia.edu>.

Unfortunately, even the conjugate Gaussian case, where fitting a GLM reduces to GP regression, naively has cubic time complexity $\mathcal{O}(N^3)$ in the number of training data N and requires $\mathcal{O}(N^2)$ memory, which is prohibitive for modern large-scale datasets. For a nonlinear link function, inference has to be done approximately, which generally exacerbates this problem. For example, inference via the Laplace approximation boils down to finding the mode of the log posterior via Newton’s method, which is equivalent to solving a *sequence* of regression problems (Spiegelhalter & Lauritzen, 1990; MacKay, 1992; Bishop, 2006).

In practice, computational resources are always limited, which for large-scale problems necessitates numerical approximations. The error incurred by scalable approximations generally affects not only the predictive accuracy of a model, but also its uncertainty quantification. Therefore the question becomes whether GLMs can be trained efficiently on large-scale data without impacting their reliability.

Recently, iterative methods have emerged which in the conjugate Gaussian case allow an explicit, tunable trade-off between reduced computation and uncertainty (Trippe et al., 2019; Wenger et al., 2022b). This computational uncertainty quantifies the inevitable approximation error in the sense of probabilistic numerics (Hennig et al., 2015; Cockayne et al., 2019b; Oates & Sullivan, 2019; Hennig et al., 2022). In this work, we take a similar approach for GLMs and importantly propose new techniques to efficiently reuse computations and reduce the necessary memory. An illustrative example of our approach, called ITERGLM, is given in Figure 1.

Contributions: In summary, we propose:

- (a) A family of efficient inference algorithms for GLMs with a tunable trade-off between computational savings and added uncertainty (Section 3).
- (b) Mechanisms to tailor the inference algorithm to a specific downstream application (Section 3.3), to optimally recycle costly computations (Section 3.4) and to restrict the memory usage, with minimal impact on inference (Section 3.5).

To demonstrate the features of our method and its efficacy we apply it to a Poisson regression problem and a large-scale classification problem (Section 5).

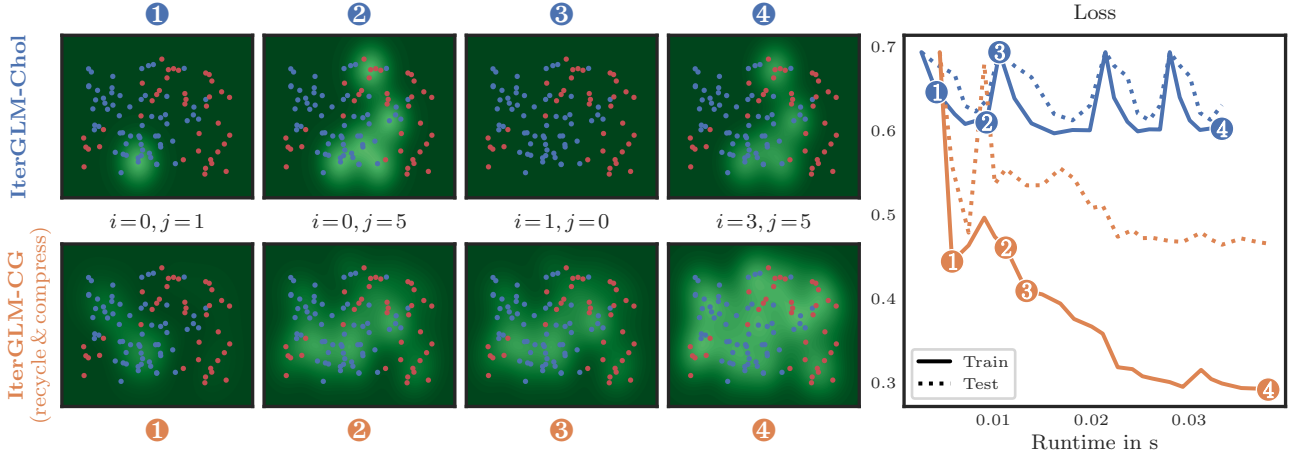


Figure 1: Binary Classification with ITERGLM. (*Top*) ITERGLM variant corresponding to the baseline approach of data subsampling and solving each regression problem exactly in each Newton step i . (*Bottom*) ITERGLM variant with a more informative policy changing how the data informs the prediction (details in Section 3.3), recycling of computations between Newton steps and compression to reduce memory. The panels show how the marginal uncertainty (■) over the latent function reduces with the number of iterations j of the iterative solver (①→②, ③→④). Using recycling, the current belief is efficiently propagated between mode-finding steps i (②→③) without performance drops (*Right*). Details in Appendix D.1.

2. Background

Let (\mathbf{X}, \mathbf{y}) be a training dataset of size N with inputs $\mathbf{X} = (\mathbf{x}_1, \dots, \mathbf{x}_N)^\top \in \mathbb{R}^{N \times D}$ and corresponding outputs $\mathbf{y} = (y_1, \dots, y_N)^\top \in \mathbb{Y}^N$, where $\mathbb{Y} = \mathbb{R}$ or $\mathbb{Y} = \mathbb{N}_0$ in the case of regression and $\mathbb{Y} = \{1, \dots, C\}$ for classification.

2.1. Generalized Linear Models (GLMs)

We consider the following probabilistic model

$$p(\mathbf{y}, \mathbf{f} | \mathbf{X}) = p(\mathbf{y} | \mathbf{f}) p(\mathbf{f} | \mathbf{X}), \quad (1)$$

where the vector $\mathbf{f} := f(\mathbf{X}) \in \mathbb{R}^{NC}$ is given by a latent function $f: \mathbb{X} \rightarrow \mathbb{R}^C$ evaluated at the training data.

Prior: Assume a multi-output Gaussian process prior¹ $\mathcal{GP}(m, K)$ over the latent function with mean function $m: \mathbb{X} \rightarrow \mathbb{R}^C$ and kernel function $K: \mathbb{X} \times \mathbb{X} \rightarrow \mathbb{R}^{C \times C}$. Therefore the latent vector has density $p(\mathbf{f} | \mathbf{X}) = \mathcal{N}(\mathbf{f}; \mathbf{m}, \mathbf{K})$ with mean $\mathbf{m} := m(\mathbf{X}) \in \mathbb{R}^{NC}$ and covariance $\mathbf{K} = K(\mathbf{X}, \mathbf{X}) \in \mathbb{R}^{NC \times NC}$ defined by N^2 blocks $K(\mathbf{x}_i, \mathbf{x}_j) \in \mathbb{R}^{C \times C}$, representing the covariance between the C latent functions evaluated at inputs \mathbf{x}_i and \mathbf{x}_j .

Likelihood: Assume iid data, which depends on the latent function via an inverse link function $\lambda: \mathbb{R}^C \rightarrow \mathbb{R}^C$, s.t.

$$p(\mathbf{y} | \mathbf{f}) = \prod_{n=1}^N p(y_n | \lambda(\mathbf{f}_n)), \quad (2)$$

where $p(y_n | \lambda(\mathbf{f}_n))$ is a log-concave likelihood, e.g.

¹Such a model is also called a Generalized GP model (GGPM) (Chan & Dong, 2011) or non-conjugate GP regression (Khan et al., 2012). See Appendix A for why we refer to this model as a GLM.

any exponential family distribution.² For example, for Poisson regression the inverse link function is given by $\lambda(f_n) = \exp(f_n)$ and for multi-class classification by $\lambda(\mathbf{f}_n) = \text{softmax}(\mathbf{f}_n)$.

For nonlinear inverse link functions, the posterior $p(f | \mathbf{X}, \mathbf{y})$ and predictive distribution $p(y_\diamond | \mathbf{X}, \mathbf{y}, \mathbf{x}_\diamond) = \int p(y_\diamond | f_\diamond) p(f_\diamond | \mathbf{X}, \mathbf{y}, \mathbf{x}_\diamond) df_\diamond$ are computationally intractable, necessitating the use of approximations.

2.2. Approximate Inference via Laplace

A popular way to perform approximate inference in a Bayesian GLM is to use a Laplace approximation (LA) (Spiegelhalter & Lauritzen, 1990; MacKay, 1992; Bishop, 2006). The idea is to approximate the posterior

$$p(\mathbf{f} | \mathbf{X}, \mathbf{y}) \approx q(\mathbf{f} | \mathbf{X}, \mathbf{y}) := \mathcal{N}(\mathbf{f}; \mathbf{f}_{\text{MAP}}, \Sigma), \quad (3)$$

with a Gaussian with mean given by the mode \mathbf{f}_{MAP} of the log posterior and covariance matrix $\Sigma := -(\nabla^2 \log p(\mathbf{f}_{\text{MAP}} | \mathbf{X}, \mathbf{y}))^{-1}$ given by the negative inverse Hessian (with respect to \mathbf{f}) at the mode.

The GLM log posterior is given up to a constant³ by

$$\begin{aligned} \Psi(\mathbf{f}) &:= \log p(\mathbf{f} | \mathbf{X}, \mathbf{y}) \\ &\stackrel{\text{c}}{=} \log p(\mathbf{y} | \mathbf{f}) + \log p(\mathbf{f} | \mathbf{X}) \\ &\stackrel{\text{c}}{=} \log p(\mathbf{y} | \mathbf{f}) - 1/2(\mathbf{f} - \mathbf{m})^\top \mathbf{K}^{-1}(\mathbf{f} - \mathbf{m}) \end{aligned} \quad (4)$$

²The Hessian of an exponential family likelihood is the negative Hessian of its log-partition function, which equals the *positive definite* covariance matrix of its sufficient statistics.

³We use $\stackrel{\text{c}}{=}$ to denote equality up to an additive constant.

due to the assumed GP prior over the latent function.

Mode-Finding via Newton’s Method: To find the mode \mathbf{f}_{MAP} , one typically uses Newton’s method, i.e.

$$\mathbf{f}_{\text{MAP}} \approx \mathbf{f}_{i+1} = \mathbf{f}_i - \nabla^2 \Psi(\mathbf{f}_i)^{-1} \cdot \nabla \Psi(\mathbf{f}_i), \quad (5)$$

$$\nabla \Psi(\mathbf{f}_i) = \nabla \log p(\mathbf{y} | \mathbf{f}_i) - \mathbf{K}^{-1}(\mathbf{f}_i - \mathbf{m}) \quad (6)$$

$$\nabla^2 \Psi(\mathbf{f}_i) = -\mathbf{W}(\mathbf{f}_i) - \mathbf{K}^{-1}. \quad (7)$$

The negative Hessian $\mathbf{W}(\mathbf{f}_i) := -\nabla^2 \log p(\mathbf{y} | \mathbf{f}_i)$ of the log likelihood at \mathbf{f}_i is positive definite for all \mathbf{f} , since we assumed a log-concave likelihood. Therefore Ψ is concave and the Newton updates are well-defined.

2.3. Prediction

Using the Laplace approximation at $\mathbf{f}_i \approx \mathbf{f}_{\text{MAP}}$ in place of the posterior, the predictive distribution for the latent function $p(f(\cdot) | \mathbf{X}, \mathbf{y}) = \int p(f(\cdot) | \mathbf{f}) q(\mathbf{f} | \mathbf{X}, \mathbf{y}) d\mathbf{f}$ is a Gaussian process $\mathcal{GP}(m_{i,*}, K_{i,*})$, with mean and covariance functions

$$m_{i,*}(\cdot) := m(\cdot) + K(\cdot, \mathbf{X})\mathbf{K}^{-1}(\mathbf{f}_{i+1} - \mathbf{m}), \quad (8)$$

$$K_{i,*}(\cdot, \cdot) := K(\cdot, \cdot) - K(\cdot, \mathbf{X})\hat{\mathbf{K}}(\mathbf{f}_i)^{-1}K(\mathbf{X}, \cdot), \quad (9)$$

where $\hat{\mathbf{K}}(\mathbf{f}_i) := \mathbf{K} + \mathbf{W}(\mathbf{f}_i)^{-1}$ (cf. Eq. 3.24; [Rasmussen & Williams, 2006](#)). We can use this predictive distribution and likelihood to compute the predictive distribution for y_\diamond at test input \mathbf{x}_\diamond . Marginalizing over $\mathbf{f}_\diamond = f(\mathbf{x}_\diamond)$, we obtain

$$p(y_\diamond | \mathbf{X}, \mathbf{y}, \mathbf{x}_\diamond) = \int p(y_\diamond | \mathbf{f}_\diamond) p(\mathbf{f}_\diamond | \mathbf{X}, \mathbf{y}, \mathbf{x}_\diamond) d\mathbf{f}_\diamond.$$

This is a C -dimensional integral which can be approximated via quadrature, MC-sampling or using specialized approximations (like the probit approximation ([MacKay, 1992](#)) in the case of a categorical likelihood and softmax inverse link function).

3. Computation-Aware Inference in GLMs

While Newton’s method typically only requires a few steps to converge for a log-concave likelihood, each step in (5) requires linear system solves with symmetric positive (semi-)definite matrices of size $NC \times NC$. Naively computing these solves numerically via Cholesky decomposition is problematic even for moderately sized datasets due to its cubic time complexity $\mathcal{O}(N^3 C^3)$ and quadratic memory requirement $\mathcal{O}(N^2 C^2)$.

3.1. Derivation of the ITERGLM Framework

We will demonstrate how to circumvent this issue by reducing the computations in exchange for increased uncertainty about the latent function. We do so by reinterpreting the Newton iteration as a sequence of GP regression problems,

solving each of these efficiently via iterative, computation-aware methods, and by recycling computation across steps, while compressing information to save memory.

Newton’s Method as Sequential GP Regression: We can interpret the Newton iteration in Equation (5) as solving a sequence of GP regression problems⁴ by rewriting the posterior $f \sim \mathcal{GP}(m_{i,*}, K_{i,*})$ at Newton step i as

$$m_{i,*}(\cdot) = m(\cdot) + K(\cdot, \mathbf{X})\hat{\mathbf{K}}(\mathbf{f}_i)^{-1}(\hat{\mathbf{y}}(\mathbf{f}_i) - \mathbf{m}) \quad (10)$$

$$K_{i,*}(\cdot, \cdot) = K(\cdot, \cdot) - \underbrace{K(\cdot, \mathbf{X})\hat{\mathbf{K}}(\mathbf{f}_i)^{-1}K(\mathbf{X}, \cdot)}_{=\mathbf{K} + \mathbf{W}(\mathbf{f}_i)^{-1}}. \quad (11)$$

where $\hat{\mathbf{y}}(\mathbf{f}_i) := \mathbf{f}_i + \mathbf{W}(\mathbf{f}_i)^{-1} \nabla \log p(\mathbf{y} | \mathbf{f}_i)$ (see [Appendix B.1](#) for a derivation). At each Newton iterate \mathbf{f}_i , Equations (10) and (11) define a GP posterior for a GP regression problem with *pseudo targets* $\hat{\mathbf{y}}(\mathbf{f}_i)$ observed with Gaussian noise $\mathcal{N}(\mathbf{0}, \mathbf{W}(\mathbf{f}_i)^{-1})$. [Figure 2](#) shows an illustration of this interpretation. If $\mathbf{W}(\mathbf{f}_i)^{-1}$ does not exist, e.g. in multi-class classification, we substitute its pseudo-inverse $\mathbf{W}(\mathbf{f}_i)^\dagger$, which for multi-class classification can be evaluated efficiently (see [Appendix B.5](#)).⁵

Computation-Aware Sequential GP Regression: Reframing the Newton iteration as sequential GP regression does not yet solve the need for linear solves with a matrix of size $NC \times NC$. However, we can leverage recent advances for GP regression. Specifically, [Wenger et al. \(2022b\)](#) propose to use a probabilistic linear solver (PLS) ([Hennig, 2015](#); [Cockayne et al., 2019a](#); [Wenger & Hennig, 2020](#)) to iteratively compute an approximate GP posterior

$$m_{i,j}(\cdot) := m(\cdot) + K(\cdot, \mathbf{X})\mathbf{v}_j \quad (12)$$

$$K_{i,j}(\cdot, \cdot) := K(\cdot, \cdot) - K(\cdot, \mathbf{X})\mathbf{C}_j K(\mathbf{X}, \cdot) \quad (13)$$

where $\mathbf{v}_j = \mathbf{C}_j(\hat{\mathbf{y}}(\mathbf{f}_i) - \mathbf{m})$. Their algorithm ITERGP, is matrix-free, i.e. it only relies on matrix-vector products $\mathbf{s} \mapsto \hat{\mathbf{K}}(\mathbf{f}_i)\mathbf{s}$, which reduces the required memory from quadratic to linear, and efficiently exploits modern parallel GPU hardware ([Charlier et al., 2021](#)). Crucially, by Theorem 2 of [Wenger et al. \(2022b\)](#), the posterior covariance in Equation (13) *exactly* quantifies the error in each approximate Newton step introduced by only using *limited computational resources*, i.e. running the linear solver for $j \ll NC$ iterations. This reduces the time complexity to $\mathcal{O}(jN^2 C^2)$. The approximate precision matrix in Equations (12) and (13),

$$\mathbf{C}_j = \mathbf{S}_j \mathbf{S}_j^\top \hat{\mathbf{K}}(\mathbf{f}_i) \mathbf{S}_j^{-1} \mathbf{S}_j^\top \xrightarrow{j \rightarrow NC} \hat{\mathbf{K}}(\mathbf{f}_i)^{-1}, \quad (14)$$

with $\mathbf{S}_j = (\mathbf{s}_1, \dots, \mathbf{s}_j) \in \mathbb{R}^{NC \times j}$ has rank j . As in ([Wenger et al., 2022b](#)), we refer to the vectors $\mathbf{s}_j \leftarrow \text{POLICY}()$ as

⁴This connection can be interpreted as a function-space viewpoint on iterative reweighted least-squares ([Holland & Welsch, 1977](#)), when applied to GLM inference.

⁵Alternatively, one can place a prior on the sum of the C latent functions ([MacKay, 1998](#), Eqn. (10)).

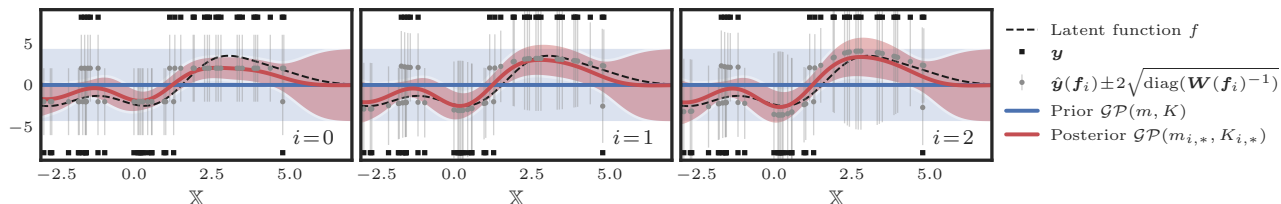


Figure 2: Approximate Inference in GLMs as Sequential GP Regression. Performing a LA at a Newton iterate f_i results in a posterior GP that coincides with the posterior to a GP regression problem with pseudo targets $\hat{y}(f_i)$ observed with Gaussian noise $\mathcal{N}(0, \mathbf{W}(f_i)^{-1})$. The plot shows an illustration of this connection for binary classification on a toy problem with the latent function drawn from a \mathcal{GP} . Notice how similar the posteriors are between Newton steps. This motivates our proposed strategy for recycling computations between steps in Section 3.4. Details in Appendix D.1.

actions defined by a user-specified *policy*. We discuss the policy choice for the GLM case in more detail in Section 3.3.

Summary: One can look at the process of finding the posterior mode f_{MAP} and the corresponding predictive distributions (Equations (8) and (9)) from different perspectives. From an optimization standpoint, we use Newton updates, each of which maximizes a local quadratic approximation of the log posterior. From a probabilistic perspective, we solve a sequence of *related* GP regression problems and ITERGP enables us to propagate a probabilistic estimate of the latent function throughout the *entire* optimization process.

3.2. Algorithm: ITERGLM

The core structure of our algorithm is an outer loop (see Algorithm 2 in Appendix C.2) of i approximate Newton steps, computed via an inner loop (see Algorithm 3 in Appendix C.3) of j PLS iterations.

For a Gaussian likelihood, the LA (Equation (3)) is exact and thus a single Newton step suffices. Our framework can therefore be regarded as a generalization of ITERGP to arbitrary log-concave likelihoods (see Theorem B.2).

New Functionality for GLM Inference: Next, we discuss the role of the policy and its potential for tailored actions for specific problems (Section 3.3). We also leverage the fact that the GP regression problems in the outer loop are related for further speedups (Section 3.4) and introduce a mechanism to control ITERGLM’s memory usage (Section 3.5).

3.3. Policy Choice: Targeted Computations

Algorithm 3 defines a *family* of inference algorithms. Its instances, defined by a concrete action policy, generally behave quite differently. To better understand what effect the sequence of actions $\mathbf{S}_j = (s_1, \dots, s_j) \in \mathbb{R}^{N_C \times j}$ has on ITERGLM, we consider the following examples.

Unit Vector Policy=Subset of Data (SoD): Choosing the actions $s_j = e_j$ to be unit vectors with all zeros except for a one at entry j , corresponds to (sequentially) condition-

ing on the first j data points in the training data in each GP regression subproblem, since $K(\cdot, \mathbf{X})\mathbf{S}_j = K(\cdot, \mathbf{X}_{1:j})$. Therefore this policy is equivalent to simply using a subset $\mathbf{X}_{1:j}$ of the data and performing *exact* GP regression (e.g. via a Cholesky decomposition) in each Newton iteration in Algorithm 2. This basic policy shows how actions *target computation* as illustrated in the top row of Figure 3.

(Conjugate) Gradient Policy: Instead of targeting individual data points, we can also specify *weighted* linear combinations of them to target the data more globally. For example, using the current residual $s_j = r_{j-1} := \hat{y}(f_i) - m - \hat{\mathbf{K}}(f_i)v_{j-1}$, approximately targets those data most, where the posterior mean prediction is far off.⁶ As Wenger et al. (2022b) show, this corresponds to using the method of conjugate gradients (CG) (Hestenes & Stiefel, 1952) to estimate the posterior mean. This policy is illustrated in the bottom row of Figure 3.

3.4. Recycling: Reusing Computations

Using ITERGP with a suitable policy for GP inference allows us to solve each GP regression problem more efficiently. However, for GLM inference we need to solve *multiple* regression problems—one per mode-finding step. Figure 2 suggests that GP posteriors across steps are highly similar. In the following, we leverage this observation to develop a novel approach, designed specifically for the GLM setting, that *efficiently recycles costly computations* between outer loop steps. See Algorithm 1 for the pseudo-code.

Core Idea: The cost of ITERGLM is dominated by repeated matrix-vector products with \mathbf{K} (see Section 3.6). However, these costly operations can be recycled and used over multiple Newton steps as we will show next. As an example, take the matrix-vector products with an action vector s in the first and second mode-finding step

$$\begin{aligned} \text{Step } i = 0: & \quad s \mapsto \hat{\mathbf{K}}(f_0)s = \mathbf{K}s + \mathbf{W}(f_0)^{-1}s \\ \text{Step } i = 1: & \quad s \mapsto \hat{\mathbf{K}}(f_1)s = \mathbf{K}s + \mathbf{W}(f_1)^{-1}s. \end{aligned}$$

⁶Since $r_{j-1} \approx \hat{y}(f_i) - m - \mathbf{K}v_{j-1} = \hat{y}(f_i) - m_{i,j-1}(\mathbf{X})$.

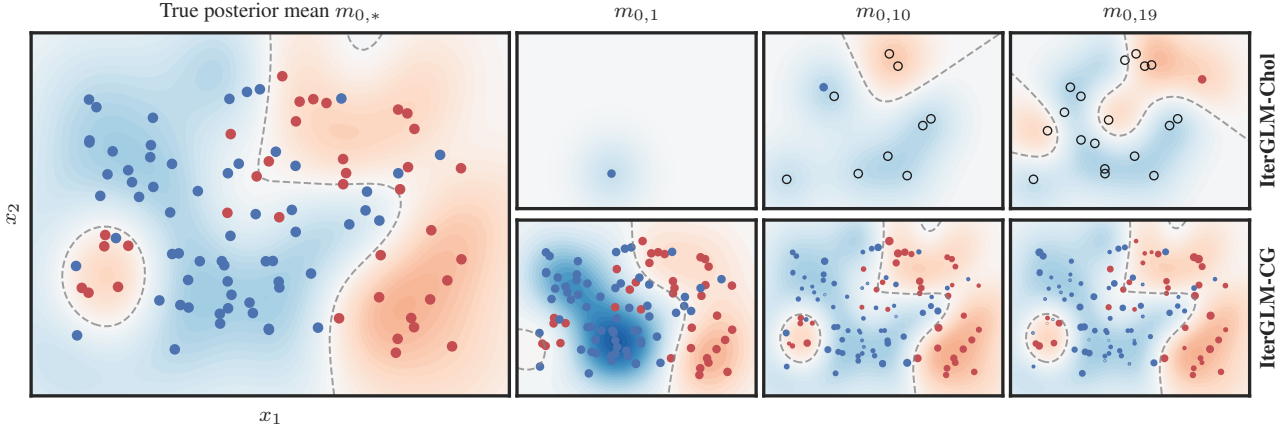


Figure 3: Different Policies of ITERGLM Applied to GP Classification. (Left) The true posterior mean $m_{0,*}$ (■) for a binary classification task (●/●) and its decision boundary (---). (Right) Current estimate of the posterior mean after 1, 10, and 19 iterations with the unit vector policy (Top) and the CG policy (Bottom). Shown are the data points selected by the policy in this iteration with the dot size indicating their relative weight. For ITERGLM-Chol, data points are targeted one by one and previously used data points are marked with (○).

Algorithm 1: Recycling: Virtual Solver Run with Optional Compression.

Input: Buffers $\mathbf{S}, \mathbf{T} \in \mathbb{R}^{N \times B}$, access to products with \mathbf{W}^{-1} , compression parameter $R \leq B$ (optional)

Output: \mathbf{C}_0 , updated buffers \mathbf{S}, \mathbf{T}

1	procedure VIRTUALSOLVERRUN($\mathbf{S}, \mathbf{T}, \mathbf{W}^{-1}$)		Time	Memory
2	$\mathbf{M} \leftarrow \mathbf{S}^\top (\mathbf{T} + \mathbf{W}^{-1} \mathbf{S})$	$\mathbf{M} = \mathbf{S}^\top (\mathbf{K} + \mathbf{W}^{-1}) \mathbf{S} \in \mathbb{R}^{B \times B}$	$\mathcal{O}(B\tau_{\mathbf{W}^{-1}} + B^2 NC)$	$\mathcal{O}(B^2)$
3	$\mathbf{U}, \mathbf{\Lambda} \leftarrow \text{ED}(\mathbf{M})$, with $\mathbf{U} = (\mathbf{u}_1, \dots, \mathbf{u}_B)$, $\mathbf{\Lambda} = \text{diag}(\lambda_1, \dots, \lambda_B) \in \mathbb{R}^{B \times B}$ and $\lambda_1 \geq \dots \geq \lambda_B$	Eigendecomposition $\mathbf{M} = \mathbf{U} \mathbf{\Lambda} \mathbf{U}^\top$	$\mathcal{O}(B^3)$	$\mathcal{O}(B^2)$
4	procedure COMPRESSION($\mathbf{U}, \mathbf{\Lambda}, R$)			
5	$\mathbf{U} \leftarrow (\mathbf{u}_1, \dots, \mathbf{u}_R)$, $\mathbf{\Lambda} \leftarrow \text{diag}(\lambda_1, \dots, \lambda_R)$	Truncate eigendecomp.		$\mathcal{O}(BR)$
6	$\mathbf{S} \leftarrow \mathbf{S} \mathbf{U}, \mathbf{T} \leftarrow \mathbf{T} \mathbf{U}$	Update buffers	$\mathcal{O}(BRNC)$	$\mathcal{O}(RNC)$
7	$\mathbf{Q}_0 \leftarrow \mathbf{S} \mathbf{\Lambda}^{-1/2}$	Construct matrix root $\mathbf{C}_0 = \mathbf{Q}_0 \mathbf{Q}_0^\top = \mathbf{S} \mathbf{\Lambda}^{-1} \mathbf{S}^\top$	$\mathcal{O}(R^2 NC)$	$\mathcal{O}(RNC)$
8	return $\mathbf{C}_0 \leftarrow \mathbf{Q}_0 \mathbf{Q}_0^\top$ and \mathbf{S}, \mathbf{T}	\mathbf{C}_0 has rank R .		

\mathbf{C}_0 is *never* formed explicitly in memory. Instead it is evaluated lazily via its root \mathbf{Q}_0 , i.e. $\mathbf{w} \mapsto \mathbf{C}_0 \mathbf{w} = \mathbf{Q}_0 (\mathbf{Q}_0^\top \mathbf{w})$.

Since \mathbf{K} is independent of \mathbf{f}_i , the product $\mathbf{K} \mathbf{s}$ is *shared* among both operations.

Virtual Solver Run: Assume we have used B action vectors $(\mathbf{s}_1, \dots, \mathbf{s}_B) =: \mathbf{S}$ in step $i=0$, and buffered the matrix-vector products $(\mathbf{K} \mathbf{s}_1, \dots, \mathbf{K} \mathbf{s}_B) = \mathbf{K} \mathbf{S} =: \mathbf{T}$. In the next Newton step $i=1$ we apply the *same* actions to a *new* linear system of equations. From Equation (14) we obtain

$$\mathbf{C} = \mathbf{S} \mathbf{M}^{-1} \mathbf{S}^\top \text{ with } \mathbf{M} := \mathbf{S}^\top \left(\underbrace{\mathbf{K} \mathbf{S}}_{=\mathbf{T}} + \mathbf{W}(\mathbf{f}_1)^{-1} \mathbf{S} \right). \quad (15)$$

So, we can *imitate* a solver run with the previous actions \mathbf{S} and construct \mathbf{C} without ever having to multiply with \mathbf{K} . The associated computational costs comprise memory for the two buffers \mathbf{S} and \mathbf{T} as well as the runtime costs for matrix-matrix products in Equation (15) and inverting \mathbf{M} . This virtual solver run is generally orders of magnitude cheaper, than running the solver from scratch with new actions (see Appendix C.4 for details). In ITERGP

(Algorithm 3), we can use this matrix as an initial estimate $\mathbf{C}_0 \leftarrow \mathbf{C}$ of the precision matrix, after which the algorithm can then be continued as usual with new actions.

The presented recycling approach can easily be extended to all Newton steps. Whenever \mathbf{K} is multiplied with an action vector, the vector itself and the resulting vector are appended to the respective buffers \mathbf{S} and \mathbf{T} . For each Newton step, an initial \mathbf{C}_0 can be constructed via Algorithm 1.

Numerical Perspective: Crucially, the above strategy does not affect the solver’s convergence properties: From a numerical linear algebra viewpoint, the strategy above is a form of *subspace recycling* (Parks et al., 2006). Specifically, \mathbf{C}_0 , as described above, defines a *deflation preconditioner* (Frank & Vuik, 2001): The projection of the initial residual $\mathbf{r}_0 = (\hat{\mathbf{y}} - \mathbf{m}) - \hat{\mathbf{K}} \mathbf{v}_0$ for the first iterate $\mathbf{v}_0 = \mathbf{C}_0 (\hat{\mathbf{y}} - \mathbf{m})$ onto the subspace $\text{span}\{\mathbf{S}\}$ spanned by the actions is zero (see Appendix B.3 for details). That means, the solution

within the subspace $\text{span}\{\mathcal{S}\}$ is already perfectly identified at initialization.

Probabilistic Perspective: Through Equation (13), we can quantify the effect of \mathcal{C}_0 on the total marginal uncertainty of the predictions at the training data $\text{Tr}(K_{i,0}(\mathbf{X}, \mathbf{X})) = \text{Tr}(\mathbf{K}) - \text{Tr}(\mathbf{K}\mathcal{C}_0\mathbf{K})$. Assuming that the observation noise $\mathbf{W}^{-1} = \mathbf{0}$ and all actions in \mathcal{S} are eigenvectors of $\hat{\mathbf{K}} = \mathbf{K}$, it simplifies to

$$\text{Tr}(K_{i,0}(\mathbf{X}, \mathbf{X})) = \text{Tr}(\mathbf{K}) - \text{Tr}(\mathbf{M}), \quad (16)$$

see Appendix B.3 for details. The second term $\text{Tr}(\mathbf{M})$ describes the *reduction* of the prior uncertainty due to \mathcal{C}_0 . It can be maximized (which is our goal) when \mathcal{S} contains those eigenvectors of $\hat{\mathbf{K}}$ with the largest eigenvalues. We take this insight as motivation for a buffer compression approach that we describe next.

3.5. Compression: Memory-Efficient Beliefs

Whenever \mathbf{K} is applied to an action vector, the buffers $\mathcal{S}, \mathcal{T} \in \mathbb{R}^{NC \times B}$ grow by NC entries. To keep memory requirements low for large-scale data, we now develop a compression strategy (see Algorithm 1).

Compression via Truncation: In Algorithm 1, $\mathbf{M}^{-1} \in \mathbb{R}^{B \times B}$ is computed via an eigendecomposition $\mathbf{M} = \mathbf{U}\mathbf{\Lambda}\mathbf{U}$, such that $\mathcal{C}_0 = \mathbf{Q}_0\mathbf{Q}_0^\top$ can be represented via its matrix root $\mathbf{Q}_0 := \mathbf{S}\mathbf{U}\mathbf{\Lambda}^{-1/2}$ for efficient storage and matrix-vector multiplies. To limit memory usage, we can use a *truncated* eigendecomposition of \mathbf{M} . Based on the intuition we gained from Equation (16), it makes sense to keep the *largest* eigenvalues (to maximize the trace) and corresponding eigenvectors. Keeping the R largest eigenvalues/-vectors yields a rank R approximation $\tilde{\mathbf{M}} = \tilde{\mathbf{U}}\tilde{\mathbf{\Lambda}}\tilde{\mathbf{U}}$ of \mathbf{M} .

Compression as Re-Weighting Actions: Forming $\mathcal{C}_0 = \mathbf{S}\tilde{\mathbf{M}}^{-1}\mathbf{S}^\top$ from the above approximation, is equivalent to a virtual solver run with the modified buffers $\tilde{\mathcal{S}} = \mathbf{S}\mathbf{U} \in \mathbb{R}^{NC \times R}$, $\tilde{\mathcal{T}} = \mathbf{K}(\mathbf{S}\mathbf{U}) = \mathbf{T}\mathbf{U} \in \mathbb{R}^{NC \times R}$ in Equation (15). This shows that the truncated eigendecomposition effectively re-weights the previous B actions to form R new ones—and the weights/linear coefficients are those eigenvectors from \mathbf{M} that maximize the uncertainty reduction. The limit R on the buffer size controls the *memory usage* as well as the rank of \mathcal{C}_0 and thereby the *expressiveness* of the associated belief as illustrated in Figure 4.

3.6. Cost Analysis of ITERGLM

The total runtime of ITERGLM is dominated by the repeated application of \mathbf{K} in Algorithm 3, i.e. $\mathcal{O}(J\tau_K)$, where J is the *total* number of solver iterations over *all* Newton steps and τ_K denotes the cost of a single matrix-vector product with \mathbf{K} . Typically, τ_K is quadratic in the number of training data points. In terms of memory, the buffers \mathcal{S}, \mathcal{T} and

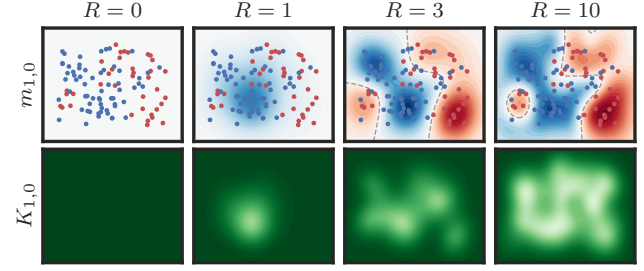


Figure 4: Compressed Beliefs. Recycled initial beliefs in the second Newton step ($i = 1$) with means $m_{1,0}$ (Top) and (co-)variance functions $K_{1,0}$ (Bottom) using compression with different buffer sizes $R \in \{0, 1, 3, 10\}$. Buffer size $R = 0$ is equivalent to not using recycling.

the matrix root \mathbf{Q} are the decisive factors with $\mathcal{O}(BNC)$. Without compression, their final size is $B = J$. Otherwise, their maximum size is given by the sum of the rank bound R and the maximum solver iterations in Algorithm 3. See Appendix C.4 for an in-depth discussion of the runtime and memory costs.

4. Related Work

The Laplace approximation (Spiegelhalter & Lauritzen, 1990; MacKay, 1992; Bishop, 2006; Rue et al., 2009) is commonly used for approximate inference in (Bayesian) GLMs. Here, we take a function-space perspective leading to a non-conjugate GP model for which a multitude of approximate methods have been proposed (e.g. Khan et al., 2012), arguably the most popular being variational approaches, such as SVGP (Titsias, 2009; Hensman et al., 2015). In contrast, to address the computational shortcomings of GLMs on large datasets we leverage iterative methods to obtain and efficiently update low-rank approximations. Iterative methods and low-rank approximations were previously used to accelerate the conjugate Gaussian special case (Cunningham et al., 2008; Murray, 2009; Guhaniyogi & Dunson, 2015; Gardner et al., 2018; Wang et al., 2019; Wenger et al., 2022a), binary classification (Zhang et al., 2014) and general Bayesian linear inverse problems (Spantini et al., 2015). Trippe et al. (2019) is closest in spirit to our approach if viewed from a weight-space perspective. Their choice of low-rank projection corresponds to a specific policy in our framework. Our approach not only enables the use of policies that are more suited to the given link function, but also saves additional computation, as well as memory, via recycling and compression. In each Newton iteration, the posterior for the current regression problem is approximated via ITERGP (Wenger et al., 2022b), which internally uses a probabilistic linear solver (Hennig, 2015; Cockayne et al., 2019a; Wenger & Hennig, 2020). Therefore, ITERGLM is a probabilistic numerical method (Hennig et al., 2015; Cockayne et al., 2019b; Oates & Sullivan, 2019; Hennig

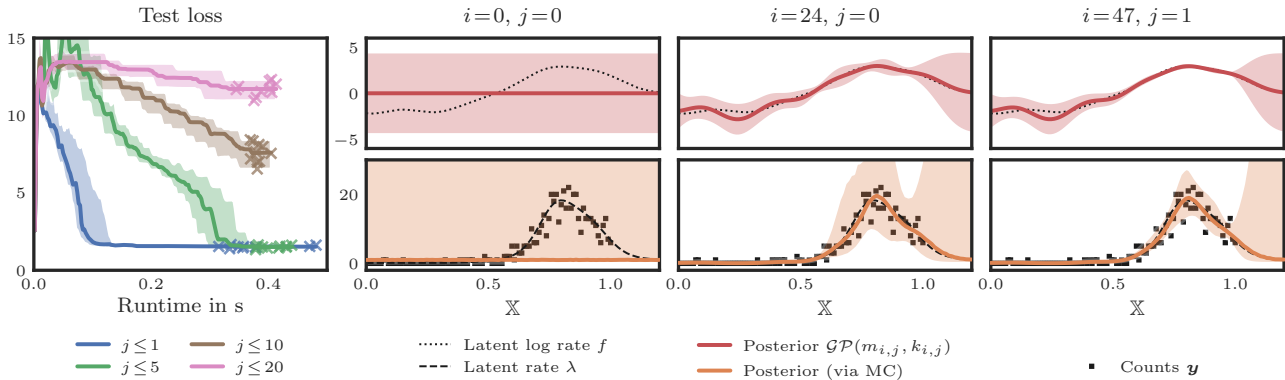


Figure 5: Poisson Regression with ITERGLM. (Left) Test loss performance for ITERGLM-CG with recycling and four schedules ($j \leq 1, 5, 10$ or 20) over 100, 20, 10 or 5 steps (always using the same total budget of 100 iterations). For each schedule, the median (solid line) and min/max (shaded area) over 10 runs are reported. The crosses indicate the end of each run. (Right) Posterior $\mathcal{GP}(m_{i,j}, k_{i,j})$ for the latent log rate f (Top) and the corresponding belief about the rate λ (Bottom) computed via MC at three timepoints during a run of ITERGLM. The shaded 95% credible intervals show how stopping early trades less computation for increased uncertainty.

et al., 2022), since it quantifies uncertainty arising from limited computation.

5. Experiments

Next, we experimentally evaluate ITERGLM. In Section 5.1, we consider Poisson regression to explore the trade-off between the number of (outer loop) mode-finding steps and (inner loop) solver iterations and in Section 5.2, we demonstrate our algorithm’s scalability and the impact of compression on performance.

5.1. Poisson Regression

Consider count data $\mathbf{y} \in \mathbb{N}_0^N$ generated from a Poisson likelihood with unknown rate $\lambda: \mathbb{X} \rightarrow \mathbb{R}_+$. The log rate f is modeled by a GP. See Appendix D.2 for details.

Data & Model: We generate a synthetic dataset by (i) sampling the log rate from a GP with an RBF kernel (ii) transforming it into the latent rate λ by exponentiation, and (iii) sampling counts $y_n \in \mathbb{N}_0$ from the Poisson distribution with rate $\lambda(\mathbf{x}_n)$. The functions f , λ , and the resulting count data are shown in Figure 5 (Right). Our GLM’s prior uses the same RBF kernel to avoid model mismatch.

Newton Steps vs. Solver Iterations: From a practical standpoint, the performance achievable within a given budget of solver iterations is highly relevant: How many linear solver iterations should be performed for each regression problem before updating the problem to maximize performance? To investigate this, we use ITERGLM-CG and distribute 100 iterations uniformly over $\{5, 10, 20, 100\}$ outer loop steps. Each run uses recycling without compression and is repeated 10 times.

Results: Figure 5 (Left) indicates that the strategy with a single iteration per step is the most efficient. An explanation could be that there is no reason to spend computational resources on an “outdated” regression problem that could be updated instead. Of course, this only applies if recycling is used, such that the *effective* number of actions accumulates. As long as $B \ll N$, the cost due to repeated recycling ($\mathcal{O}(N)$) is dwarfed by the cost of products with \mathbf{K} ($\mathcal{O}(N^2)$). Figure 5 (Right) shows an ITERGLM-CG run with one iteration per step. As we spend more computational resources, our estimates approach the underlying latent function and, where data is available, the uncertainty contracts.

5.2. Large-Scale GP Multi-Class Classification

Next, we showcase ITERGLM’s scalability on a GP classification problem. See Appendix D.3 for details.

Data & Model: We generate $N = 10^5$ data points from a Gaussian mixture model with $C = 10$ classes. We use the softmax likelihood and assume independent GPs (each equipped with a Matérn($\frac{3}{2}$) kernel) for the C outputs of the latent function. While this experiment uses synthetic data, the latent function is *not* drawn from the assumed GP model and thus the kernel is *not* perfectly identified. Also note that, if we formed $\hat{\mathbf{K}}$ in (working) memory explicitly, this would require $(NC)^2 \cdot 8 \text{ byte} = 8000 \text{ GB}$ (in double precision). Solving the linear systems *precisely*, e.g. via Cholesky decomposition, is therefore infeasible, whereas our family of methods is matrix-free and can still be applied.

Methods: We compare the subset of data (SoD) approach from Section 3.3, the popular variational approximation SVGP (Titsias, 2009; Hensman et al., 2015) and ITERGLM-CG. For SoD, we materialize $\hat{\mathbf{K}}$ in memory and compute

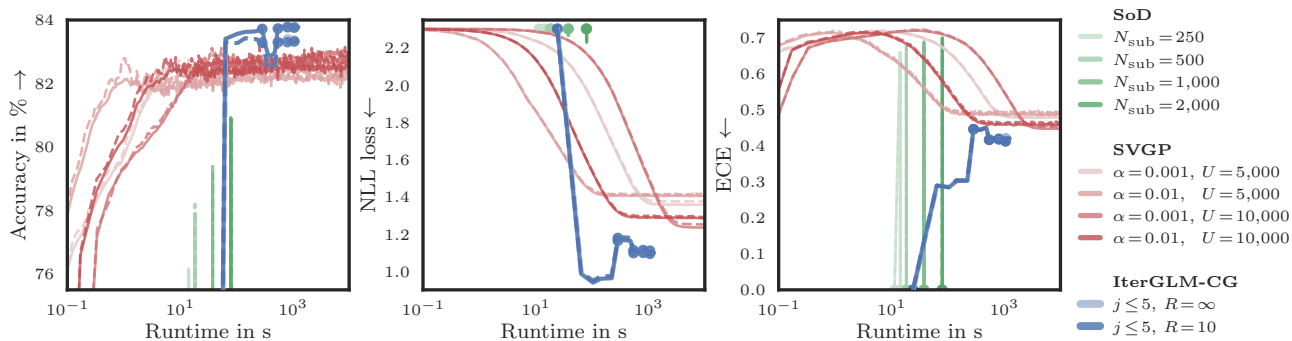


Figure 6: Large-Scale GP Classification. Comparison of SoD with $N_{\text{sub}} \in \{250, 500, 1000, 2000\}$, SVGP with learning rate $\alpha \in \{0.001, 0.01, 0.05\}$ and $U \in \{1000, 2500, 5000, 10000\}$ inducing points (only the best four runs are reported) and ITERGLM-CG with buffer size $R \in \{\infty, 10\}$ on a classification problem with $N = 10^5$ training data points and $C = 10$ classes in terms of accuracy (Left), NLL loss (Center) and ECE (Right). Training metrics are shown as solid, test metrics as dashed lines. For SoD and ITERGLM-CG, circles indicate the start of an outer loop iteration. ITERGLM-CG performs best both in terms of accuracy and uncertainty quantification (measured via NLL and ECE) with minimal memory requirements.

its Cholesky decomposition. Four different subset sizes are used—the largest one $N_{\text{sub}} = 2000$ requires 3.2 GB of memory for \hat{K} . As additional baseline, we use GPYTORCH’s (Gardner et al., 2018) SVGP implementation. We optimize the ELBO for 10^4 seconds using ADAM with batch size = 1024. The learning rate α and the number of inducing points U are tuned via grid search. ITERGLM-CG is applied to the *full* training set with recycling and $R \in \{\infty, 10\}$. The number of solver iterations is limited by $j \leq 5$. We use KEOPS (Charlier et al., 2021) and GPYTORCH for fast kernel-matrix multiplies. For this work, we consider kernel hyperparameter optimization out of scope—all methods therefore use the same fixed hyperparameters. The benchmark is run on one NVIDIA Tesla V100-SXM2-32GB GPU.

Results: Figure 6: Once the matrix is formed in memory, the SoD approaches are very fast—even with $N_{\text{sub}} = 2000$, they converge within 100 s (all SoD runs only require two Newton steps). With increasing N_{sub} , the runs reach higher accuracy at the cost of increased memory requirements. With SVGP, increasing the number of inducing points consistently improves performance at the cost of slower training. Increasing the learning rate to compensate for that results in instabilities—the respective runs do not exhibit competitive performance. Both SoD and SVGP fall short of ITERGLM-CG in all three performance metrics. Using recycling, ITERGLM-CG maintains low loss/high accuracy throughout training, even when compression is used. It reaches the lowest final expected calibration error (ECE)⁷ (indicating better uncertainty quantification), is more memory-efficient than SoD (especially with compression) and, in contrast to SVGP, does not require extensive tuning.

⁷Small ECE on its own is *not* conclusive. For example, all methods initially predict using the prior, which assigns uniform probability across classes. Therefore all classifiers are calibrated at initialization (ECE = 0), but they perform no better than random.

6. Conclusion

GLMs provide a flexible probabilistic framework encompassing, among others, GP regression, GP classification and Poisson regression. Training GLMs on large datasets, however, necessitates approximations. Our method ITERGLM quantifies and continuously propagates the errors caused by these approximations, in the form of uncertainty. The information collected during training is efficiently recycled and compressed, reducing runtime and memory requirements.

A limitation of our approach is directly inherited from the Laplace approximation: If the initial linearization point (the GP prior mean) is not representative, the resulting uncertainty can be over- or underestimated. A simple, albeit perhaps not perfectly satisfying remedy is to choose reasonable or cautious priors in practice.

So far, we have only explored the policy design space in a limited fashion. The policy controls which areas of the data space are targeted and accounted for in the posterior. Tailoring the actions to the *specific* problem could further increase our method’s efficiency. For example, for classification problems, a good strategy might be not to spend computational resources on data points where the prediction is already definitive.

Finally, a promising application for ITERGLM may be Bayesian deep learning. A popular approach to equip a neural net with uncertainty is via a Laplace approximation (MacKay, 1991; Ritter et al., 2018; Khan et al., 2019), which is equivalent to a GP classification problem with a neural tangent kernel prior (Jacot et al., 2018; Immer et al., 2021). There, the SoD approach is regularly used (Immer et al., 2021, Sec. A2.2), for which our approach might offer significant improvements.

Broader Impact

This paper proposes a novel method for approximate inference in a flexible and widely-used model class. By re-using costly computations and compressing information, our method aims at reducing computational cost which can ideally reduce the environmental impact of deploying such models. Since our paper is dedicated to a fundamental problem class with a wide range of applications, misuse of our method for ethically reprehensible applications cannot be ruled out.

Acknowledgements

The authors gratefully acknowledge financial support by the DFG through Project HE 7114/5-1 in SPP2298/1, the DFG Cluster of Excellence “Machine Learning - New Perspectives for Science”, EXC 2064/1, project number 390727645; the German Federal Ministry of Education and Research (BMBF) through the Tübingen AI Center (FKZ:01IS18039A); and funds from the Ministry of Science, Research and Arts of the State of Baden-Württemberg. Lukas Tatzel is grateful to the International Max Planck Research School for Intelligent Systems (IMPRS-IS) for support. Jonathan Wenger was supported by the Gatsby Charitable Foundation (GAT3708), the Simons Foundation (542963) and the Kavli Foundation. Frank Schneider is supported by funds from the Cyber Valley Research Fund.

References

- Bishop, C. M. *Pattern Recognition and Machine Learning*. Springer, 2006.
- Chan, A. B. and Dong, D. Generalized Gaussian process models. In *Conference on Computer Vision and Pattern Recognition (CVPR)*, 2011. doi: 10.1109/CVPR.2011.5995688.
- Charlier, B., Feydy, J., Glaunès, J. A., Collin, F.-D., and Durif, G. Kernel operations on the GPU, with autodiff, without memory overflows. *Journal of Machine Learning Research*, 22(74):1–6, 2021. URL <http://jmlr.org/papers/v22/20-275.html>.
- Cockayne, J., Oates, C., Ipsen, I. C., and Girolami, M. A Bayesian conjugate gradient method. *Bayesian Analysis*, 14(3):937–1012, 2019a.
- Cockayne, J., Oates, C., Sullivan, T. J., and Girolami, M. Bayesian probabilistic numerical methods. *SIAM Review*, 61(4):756–789, 2019b.
- Cunningham, J. P., Shenoy, K. V., and Sahani, M. Fast Gaussian process methods for point process intensity estimation. In *International Conference on Machine Learning (ICML)*, 2008.
- Detlefsen, N. S., Borovec, J., Schock, J., Jha, A. H., Koker, T., Di Liello, L., Stancl, D., Quan, C., Grechkin, M., and Falcon, W. TorchMetrics - measuring reproducibility in PyTorch. *Journal of Open Source Software*, 7(70):4101, 2022.
- Dobson, A. J. and Barnett, A. G. *An Introduction to Generalized Linear Models*. CRC press, 2018.
- Frank, J. and Vuik, C. On the construction of deflation-based preconditioners. *SIAM Journal on Scientific Computing*, 23(2):442–462, 2001.
- Gardner, J. R., Pleiss, G., Bindel, D., Weinberger, K. Q., and Wilson, A. G. GPyTorch: Blackbox matrix-matrix Gaussian process inference with GPU acceleration. In *Advances in Neural Information Processing Systems (NeurIPS)*, 2018.
- Guhaniyogi, R. and Dunson, D. B. Bayesian compressed regression. *Journal of the American Statistical Association*, 110(512):1500–1514, 2015. doi: 10.1080/01621459.2014.969425. URL <https://doi.org/10.1080/01621459.2014.969425>.
- Hennig, P. Probabilistic interpretation of linear solvers. *SIAM Journal on Optimization*, 25(1):234–260, 2015.
- Hennig, P., Osborne, M. A., and Girolami, M. Probabilistic numerics and uncertainty in computations. *Proceedings of the Royal Society of London A: Mathematical, Physical and Engineering Sciences*, 471(2179), 2015.
- Hennig, P., Osborne, M. A., and Kersting, H. P. *Probabilistic Numerics: Computation as Machine Learning*. Cambridge University Press, 2022. ISBN 9781316681411. doi: 10.1017/9781316681411.
- Hensman, J., Matthews, A., and Ghahramani, Z. Scalable Variational Gaussian Process Classification. In *International Conference on Artificial Intelligence and Statistics (AISTATS)*, 2015. URL <https://proceedings.mlr.press/v38/hensman15.html>.
- Hestenes, M. R. and Stiefel, E. Methods of conjugate gradients for solving linear systems. *Journal of Research of the National Bureau of Standards*, 49, 1952.
- Holland, P. W. and Welsch, R. E. Robust regression using iteratively reweighted least-squares. *Communications in Statistics-theory and Methods*, 6(9):813–827, 1977.
- Immer, A., Korzepa, M., and Bauer, M. Improving predictions of Bayesian neural nets via local linearization, 2021.
- Jacot, A., Gabriel, F., and Hongler, C. Neural tangent kernel: Convergence and generalization in neural networks.

- In *Advances in Neural Information Processing Systems (NeurIPS)*, 2018. URL <http://arxiv.org/abs/1806.07572>.
- Khan, E., Mohamed, S., and Murphy, K. P. Fast Bayesian Inference for Non-Conjugate Gaussian Process Regression. In *Advances in Neural Information Processing Systems (NeurIPS)*, volume 25, 2012.
- Khan, M. E., Immer, A., Abedi, E., and Korzepa, M. Approximate inference turns deep networks into gaussian processes. In *Advances in Neural Information Processing Systems (NeurIPS)*, 2019. URL <http://arxiv.org/abs/1906.01930>.
- Kumar, A., Liang, P. S., and Ma, T. Verified uncertainty calibration. In *Advances in Neural Information Processing Systems (NeurIPS)*, 2019.
- MacKay, D. Bayesian model comparison and backprop nets. In *Advances in Neural Information Processing Systems (NeurIPS)*, 1991.
- MacKay, D. J. Choice of basis for laplace approximation. *Machine Learning*, 33(1):77–86, 1998. ISSN 1573-0565. doi: 10.1023/A:1007558615313.
- MacKay, D. J. C. The evidence framework applied to classification networks. *Neural Computation*, 4(5):720–736, 1992. doi: 10.1162/neco.1992.4.5.720.
- Murray, I. Gaussian processes and fast matrix-vector multiplies. In *Numerical Mathematics in Machine Learning Workshop (ICML)*, 2009.
- Nelder, J. A. and Wedderburn, R. W. M. Generalized linear models. *Journal of the Royal Statistical Society. Series A (General)*, 135(3):370–384, 1972.
- Oates, C. and Sullivan, T. J. A modern retrospective on probabilistic numerics. *Statistics and Computing*, 2019.
- Parks, M. L., Sturler, E. d., Mackey, G., Johnson, D. D., and Maiti, S. Recycling krylov subspaces for sequences of linear systems. *SIAM Journal on Scientific Computing*, 2006. doi: 10.1137/040607277. URL <https://epubs.siam.org/doi/10.1137/040607277>.
- Paszke, A., Gross, S., Massa, F., Lerer, A., Bradbury, J., Chanan, G., Killeen, T., Lin, Z., Gimelshein, N., Antiga, L., Desmaison, A., Kopf, A., Yang, E., DeVito, Z., Raison, M., Tejani, A., Chilamkurthy, S., Steiner, B., Fang, L., Bai, J., and Chintala, S. PyTorch: An imperative style, high-performance deep learning library. In *Advances in Neural Information Processing Systems (NeurIPS)*, 2019.
- Rasmussen, C. E. and Williams, C. K. I. *Gaussian Processes for Machine Learning*. MIT Press, 2006.
- Ritter, H., Botev, A., and Barber, D. A scalable laplace approximation for neural networks. In *International Conference on Learning Representations (ICLR)*, 2018. URL <https://openreview.net/forum?id=Skdvd2xAZ>.
- Rue, H., Martino, S., and Chopin, N. Approximate Bayesian inference for latent Gaussian models by using integrated nested Laplace approximations. *Journal of the Royal Statistical Society: Series B (Statistical Methodology)*, 71(2):319–392, 2009. ISSN 1467-9868. doi: 10.1111/j.1467-9868.2008.00700.x.
- Spantini, A., Solonen, A., Cui, T., Martin, J., Tenorio, L., and Marzouk, Y. Optimal low-rank approximations of Bayesian linear inverse problems. *SIAM Journal on Scientific Computing*, 37(6), 2015. doi: 10.1137/140977308. URL <http://arxiv.org/abs/1407.3463>.
- Spiegelhalter, D. J. and Lauritzen, S. L. Sequential updating of conditional probabilities on directed graphical structures. *Networks*, 20(5):579–605, 1990. doi: <https://doi.org/10.1002/net.3230200507>.
- Titsias, M. Variational learning of inducing variables in sparse Gaussian processes. In *International Conference on Artificial Intelligence and Statistics (AISTATS)*, 2009.
- Trippe, B. L., Huggins, J. H., Agrawal, R., and Broderick, T. LR-GLM: High-dimensional Bayesian inference using low-rank data approximations. In *International Conference on Machine Learning (ICML)*, 2019. doi: 10.48550/arXiv.1905.07499. URL <http://arxiv.org/abs/1905.07499>.
- Wang, K. A., Pleiss, G., Gardner, J. R., Tyree, S., Weinberger, K. Q., and Wilson, A. G. Exact Gaussian processes on a million data points. *Advances in Neural Information Processing Systems (NeurIPS)*, 32, 2019.
- Wenger, J. and Hennig, P. Probabilistic linear solvers for machine learning. In *Advances in Neural Information Processing Systems (NeurIPS)*, 2020.
- Wenger, J., Pleiss, G., Hennig, P., Cunningham, J. P., and Gardner, J. R. Preconditioning for scalable Gaussian process hyperparameter optimization. In *International Conference on Machine Learning (ICML)*, 2022a. URL <https://arxiv.org/abs/2107.00243>.
- Wenger, J., Pleiss, G., Pförtner, M., Hennig, P., and Cunningham, J. P. Posterior and computational uncertainty in Gaussian processes. In *Advances in Neural Information Processing Systems (NeurIPS)*, 2022b. URL <https://arxiv.org/abs/2205.15449>.

Zhang, L., Mahdavi, M., Jin, R., Yang, T., and Zhu, S. Random projections for classification: A recovery approach. *IEEE Transactions on Information Theory*, 60(11):7300–7316, 2014. doi: 10.1109/TIT.2014.2359204.

Accelerating Generalized Linear Models by Trading off Computation for Uncertainty

Supplementary Materials

The supplementary materials contain derivations for our theoretical framework and proofs for the mathematical statements in the main text. We also provide implementation specifics and describe our experimental setup in more detail.

A Terminology GLM vs. GGPM vs. Non-Conjugate GP	13
B Mathematical Details	13
B.1 Newton’s Method as Sequential GP Regression	13
B.2 Our Algorithm is an Extension of ITERGP	14
B.3 Virtual Solver Run	15
B.4 Derivatives of the Poisson Log Likelihood	16
B.5 Pseudo-Inverse of Negative Hessian of the Log Likelihood for Multi-Class Classification	17
C Implementation Details	18
C.1 Ordering within Vectors & Matrices	18
C.2 ITERGLM Outer Loop	19
C.3 ITERGLM Inner Loop: ITERGP with a Virtual Solver Run	19
C.4 Cost Analysis of ITERGLM	19
C.4.1 Matrix-Vector Products	20
C.4.2 Cost Analysis Algorithms 1, 2 and 3	21
D Experimental Details	21
D.1 Binary Classification	21
D.2 Poisson Regression	22
D.3 Large-Scale GP Multi-Class Classification	23

A. Terminology GLM vs. GGPM vs. Non-Conjugate GP

We chose to use the term “generalized linear model” (GLM) to refer to members of the model class described in Section 2.1 because the latent GP $f \sim \mathcal{GP}(0, K)$ can be equivalently viewed as a linear model $f(\mathbf{x}) = \phi(\mathbf{x})^\top \mathbf{v} = k(\mathbf{x}, \mathbf{X})\mathbf{v}$ with parameters given by the representer weights $\mathbf{v} = \hat{\mathbf{K}}^{-1}\hat{\mathbf{y}}$ and feature functions $\phi(\cdot)^\top = k(\cdot, \mathbf{X})$. Note that this directly extends to the case of a non-zero prior mean function by simply subtracting the prior mean from the data. This model also encompasses the “textbook” Bayesian GLM with a latent linear function $f(\mathbf{x}) = \varphi(\mathbf{x})^\top \mathbf{w}$ and prior $\mathbf{w} \sim \mathcal{N}(0, \Sigma)$ by choosing a kernel of the form $K(\mathbf{x}_0, \mathbf{x}_1) = \varphi(\mathbf{x}_0)^\top \Sigma \varphi(\mathbf{x}_1)$ (see Sec. 2.1.2 & 2.2 of Rasmussen & Williams (2006)). Therefore the use of the terminology “generalized linear model” encompasses both the classic formulation of the model (Nelder & Wedderburn, 1972) in weight space and its modern function-space generalization using a Gaussian process prior over the latent function (e.g. Chan & Dong, 2011; Khan et al., 2012; Hensman et al., 2015).

B. Mathematical Details

B.1. Newton’s Method as Sequential GP Regression

In Section 3.1, we reinterpret the Newton iteration as a sequence of GP regression problems. More specifically, we rewrite the posterior predictive mean (Equation (8)) as a GP posterior for a regression problem (Equation (10)). Here, we provide a proof for this connection.

Proposition B.1 (Reformulation of the Newton Step)

Let $\mathbf{W}(\mathbf{f}_i)$ be invertible. Using the transform $\mathbf{g} := \mathbf{f} - \mathbf{m}$ and consequently $\mathbf{g}_i = \mathbf{f}_i - \mathbf{m}$, the Newton step (Equation (5)) can be written as

$$\mathbf{g}_{i+1} = \mathbf{K}(\mathbf{K} + \mathbf{W}(\mathbf{f}_i)^{-1})^{-1} (\mathbf{g}_i + \mathbf{W}(\mathbf{f}_i)^{-1} \nabla \log p(\mathbf{y} | \mathbf{f}_i)).$$

Proof. Recall from Equations (5) to (7) that

$$\begin{aligned} \mathbf{f}_{i+1} &= \mathbf{f}_i - \nabla^2 \Psi(\mathbf{f}_i)^{-1} \cdot \nabla \Psi(\mathbf{f}_i), \quad \text{with} \quad \nabla \Psi(\mathbf{f}_i) = \nabla \log p(\mathbf{y} | \mathbf{f}_i) - \mathbf{K}^{-1}(\mathbf{f}_i - \mathbf{m}) \\ &\quad \nabla^2 \Psi(\mathbf{f}_i) = -\mathbf{W}(\mathbf{f}_i) - \mathbf{K}^{-1}, \end{aligned}$$

where $\mathbf{W}(\mathbf{f}_i) = -\nabla^2 \log p(\mathbf{y} | \mathbf{f}_i)$ denotes the negative Hessian (with respect to \mathbf{f}) of the log likelihood evaluated at \mathbf{f}_i . It holds

$$\begin{aligned} \mathbf{f}_{i+1} &= \mathbf{f}_i - \nabla^2 \Psi(\mathbf{f}_i)^{-1} \cdot \nabla \Psi(\mathbf{f}_i) \\ &= \mathbf{f}_i + (\mathbf{W}(\mathbf{f}_i) + \mathbf{K}^{-1})^{-1} \cdot (\nabla \log p(\mathbf{y} | \mathbf{f}_i) - \mathbf{K}^{-1}(\mathbf{f}_i - \mathbf{m})) \end{aligned}$$

By subtracting \mathbf{m} from both sides we obtain

$$\begin{aligned} \mathbf{g}_{i+1} &= \mathbf{g}_i + (\mathbf{W}(\mathbf{f}_i) + \mathbf{K}^{-1})^{-1} \cdot (\nabla \log p(\mathbf{y} | \mathbf{f}_i) - \mathbf{K}^{-1}\mathbf{g}_i) \\ &= (\mathbf{W}(\mathbf{f}_i) + \mathbf{K}^{-1})^{-1} ((\mathbf{W}(\mathbf{f}_i) + \mathbf{K}^{-1})\mathbf{g}_i + \nabla \log p(\mathbf{y} | \mathbf{f}_i) - \mathbf{K}^{-1}\mathbf{g}_i) \\ &= (\mathbf{W}(\mathbf{f}_i) + \mathbf{K}^{-1})^{-1} (\mathbf{W}(\mathbf{f}_i)\mathbf{g}_i + \nabla \log p(\mathbf{y} | \mathbf{f}_i)) \\ &= (\mathbf{W}(\mathbf{f}_i) + \mathbf{K}^{-1})^{-1} \mathbf{W}(\mathbf{f}_i) (\mathbf{g}_i + \mathbf{W}(\mathbf{f}_i)^{-1} \nabla \log p(\mathbf{y} | \mathbf{f}_i)) \\ &= (\mathbf{I} + \mathbf{W}(\mathbf{f}_i)^{-1} \mathbf{K}^{-1})^{-1} (\mathbf{g}_i + \mathbf{W}(\mathbf{f}_i)^{-1} \nabla \log p(\mathbf{y} | \mathbf{f}_i)) \\ &= (\mathbf{K}\mathbf{K}^{-1} + \mathbf{W}(\mathbf{f}_i)^{-1} \mathbf{K}^{-1})^{-1} (\mathbf{g}_i + \mathbf{W}(\mathbf{f}_i)^{-1} \nabla \log p(\mathbf{y} | \mathbf{f}_i)) \\ &= \mathbf{K}(\mathbf{K} + \mathbf{W}(\mathbf{f}_i)^{-1})^{-1} (\mathbf{g}_i + \mathbf{W}(\mathbf{f}_i)^{-1} \nabla \log p(\mathbf{y} | \mathbf{f}_i)) \\ &= \mathbf{K}\hat{\mathbf{K}}(\mathbf{f}_i)^{-1} (\mathbf{g}_i + \mathbf{W}(\mathbf{f}_i)^{-1} \nabla \log p(\mathbf{y} | \mathbf{f}_i)), \end{aligned}$$

with $\hat{\mathbf{K}}(\mathbf{f}_i) := \mathbf{K} + \mathbf{W}(\mathbf{f}_i)^{-1}$. □

Newton’s Method as Sequential GP Regression: Using the LA at \mathbf{f}_i , we obtain a GP posterior (see Equations (8) and (9))

in Section 2). With Proposition B.1 (i.e. assuming that $\mathbf{W}(\mathbf{f}_i)^{-1}$ exists), we can rewrite Equation (8) as

$$\begin{aligned}
 m_{i,*}(\cdot) &= m(\cdot) + K(\cdot, \mathbf{X})\mathbf{K}^{-1}(\mathbf{f}_{i+1} - \mathbf{m}) \\
 &= m(\cdot) + K(\cdot, \mathbf{X})\mathbf{K}^{-1}\mathbf{g}_{i+1} \\
 &= m(\cdot) + K(\cdot, \mathbf{X})\mathbf{K}^{-1}\mathbf{K}\hat{\mathbf{K}}(\mathbf{f}_i)^{-1}(\mathbf{g}_i + \mathbf{W}(\mathbf{f}_i)^{-1}\nabla \log p(\mathbf{y} | \mathbf{f}_i)) \\
 &= m(\cdot) + K(\cdot, \mathbf{X})\hat{\mathbf{K}}(\mathbf{f}_i)^{-1}(\mathbf{f}_i + \mathbf{W}(\mathbf{f}_i)^{-1}\nabla \log p(\mathbf{y} | \mathbf{f}_i) - \mathbf{m}) \\
 &= m(\cdot) + K(\cdot, \mathbf{X})\hat{\mathbf{K}}(\mathbf{f}_i)^{-1}(\hat{\mathbf{y}}(\mathbf{f}_i) - \mathbf{m}),
 \end{aligned}$$

where $\hat{\mathbf{y}}(\mathbf{f}_i) := \mathbf{f}_i + \mathbf{W}(\mathbf{f}_i)^{-1}\nabla \log p(\mathbf{y} | \mathbf{f}_i)$. This proves Equation (10). Together with Equation (9), $m_{i,*}$ defines a GP posterior for a GP regression problem with pseudo targets $\hat{\mathbf{y}}(\mathbf{f}_i)$ observed with Gaussian noise $\mathcal{N}(\mathbf{0}, \mathbf{W}(\mathbf{f}_i)^{-1})$ (Rasmussen & Williams, 2006, Eqs. (2.24) and (2.38)).

Equation (10) requires solving the linear system $\hat{\mathbf{K}}(\mathbf{f}_i) \cdot \mathbf{v} = \hat{\mathbf{y}}(\mathbf{f}_i) - \mathbf{m}$ of size NC . Then, $m_{i,*}(\cdot) = m(\cdot) + K(\cdot, \mathbf{X})\mathbf{v}$. In Proposition B.1, we can write \mathbf{g}_{i+1} as $\mathbf{g}_{i+1} = \mathbf{K}\mathbf{v}$, i.e. $\mathbf{f}_{i+1} = \mathbf{K}\mathbf{v} + \mathbf{m}$. So, both the predictive mean $m_{i,*}$ and the Newton update \mathbf{f}_{i+1} follow directly from the solution \mathbf{v} . In that sense, performing inference and computing Newton iterates are equivalent.

What If $\mathbf{W}(\mathbf{f}_i)$ Is Not Invertible? For multi-class classification, \mathbf{W} has rank $N(C - 1)$ and thus \mathbf{W}^{-1} does not exist. Therefore, we use its pseudo-inverse \mathbf{W}^\dagger instead. We derive an explicit expression for \mathbf{W}^\dagger in Appendix B.5 which allows for efficient matrix-vector multiplies.

B.2. Our Algorithm is an Extension of ITERGP

Our algorithm ITERGLM uses ITERGP as a core building block. ITERGLM's outer loop (Algorithm 2) can be understood as a sequence of GP regression problems and we use ITERGP (that implements the inner loop, see Algorithm 3) for finding approximate solutions to each of these problems. In the case of GP regression (i.e. with a Gaussian likelihood), the outer loop collapses to a *single* iteration and ITERGLM coincides exactly with ITERGP, as we show in the following.

Theorem B.2 (Generalization of ITERGP)

For a Gaussian likelihood $p(\mathbf{y} | \mathbf{f}) = \mathcal{N}(\mathbf{y}; \mathbf{f}, \mathbf{\Lambda})$, ITERGLM converges in a single Newton step (i.e. $\mathbf{f}_1 = \mathbf{f}_{\text{MAP}}$) and ITERGLM (Algorithm 2) coincides exactly with ITERGP (Algorithm 3).

Proof. Since the likelihood is Gaussian $p(\mathbf{y} | \mathbf{f}) = \mathcal{N}(\mathbf{y}; \mathbf{f}, \mathbf{\Lambda})$, the log likelihood is given by

$$\log p(\mathbf{y} | \mathbf{f}) \stackrel{c}{=} -\frac{1}{2}(\mathbf{f} - \mathbf{y})^\top \mathbf{\Lambda}^{-1}(\mathbf{f} - \mathbf{y}).$$

This gives rise to a log posterior (Equation (4))

$$\begin{aligned}
 \Psi(\mathbf{f}) &:= \log p(\mathbf{f} | \mathbf{X}, \mathbf{y}) \\
 &\stackrel{c}{=} \log p(\mathbf{y} | \mathbf{f}) - \frac{1}{2}(\mathbf{f} - \mathbf{m})^\top \mathbf{K}^{-1}(\mathbf{f} - \mathbf{m}) \\
 &= -\frac{1}{2}(\mathbf{f} - \mathbf{y})^\top \mathbf{\Lambda}^{-1}(\mathbf{f} - \mathbf{y}) - \frac{1}{2}(\mathbf{f} - \mathbf{m})^\top \mathbf{K}^{-1}(\mathbf{f} - \mathbf{m})
 \end{aligned}$$

that is *quadratic* in \mathbf{f} . The first Newton iterate \mathbf{f}_1 therefore coincides with log posterior's maximizer $\mathbf{f}_1 = \mathbf{f}_{\text{MAP}}$. The outer loop of ITERGLM thus reduces to a single iteration.

How does this step look from the perspective of the ITERGLM algorithm? First note that $\mathbf{W}(\mathbf{f}) = -\nabla^2 \log p(\mathbf{y} | \mathbf{f}) \equiv \mathbf{\Lambda}^{-1}$. Given an initial \mathbf{f}_0 , ITERGLM computes the observation noise $\mathbf{W}^{-1}(\mathbf{f}_0) = \mathbf{\Lambda}$ and pseudo regression targets $\hat{\mathbf{y}}(\mathbf{f}_0) = \mathbf{f}_0 + \mathbf{W}(\mathbf{f}_0)^{-1}\nabla \log p(\mathbf{y} | \mathbf{f}_0) = \mathbf{f}_0 - \mathbf{\Lambda}\mathbf{\Lambda}^{-1}(\mathbf{f}_0 - \mathbf{y}) = \mathbf{y}$. Both these quantities are *independent* of the initialization \mathbf{f}_0 . Thus, the first (and only) regression problem that ITERGLM forms in the outer loop is the *original* regression problem (defined by labels \mathbf{y} and the observation noise $\mathbf{\Lambda}$) and ITERGP is applied to solve that regression problem. This shows that our framework recovers ITERGP in the case of a Gaussian likelihood and our algorithm can thus be regarded as an extension thereof. \square

B.3. Virtual Solver Run

In Section 3.4, we showed that it is possible to *imitate* a solver run using the *previous* actions on the *new* problem, without ever having to multiply by \hat{K} . The pseudo code is given in Algorithm 1. Here, we discuss the numerical and probabilistic perspective on that procedure in more detail and provide derivations for the statements in the main text.

Numerical Perspective: Let $\mathbf{S} = (s_1, \dots, s_B)$ the matrix of stacked linearly independent actions. We use $\mathbf{C}_0 = \mathbf{S}(\mathbf{S}^\top \hat{\mathbf{K}} \mathbf{S})^{-1} \mathbf{S}^\top$ (see Equation (14)) as an initial estimate of the precision matrix in Algorithm 3. The corresponding initial residual (see Algorithm 3) $\mathbf{r}_0 = (\hat{\mathbf{y}} - \mathbf{m}) - \hat{\mathbf{K}} \mathbf{v}_0$ for the first iterate $\mathbf{v}_0 = \mathbf{C}_0(\hat{\mathbf{y}} - \mathbf{m})$ can be decomposed into $\mathbf{P}_S \mathbf{r}_0$ and $(\mathbf{I} - \mathbf{P}_S) \mathbf{r}_0$. $\mathbf{P}_S = \mathbf{S}(\mathbf{S}^\top \mathbf{S})^{-1} \mathbf{S}^\top$ is the orthogonal projection onto the subspace $\text{span}\{\mathbf{S}\}$ spanned by the actions.

Proposition B.3 (Residual in $\text{span}\{\mathbf{S}\}$ Is Zero)

The orthogonal projection $\mathbf{P}_S \mathbf{r}_0$ of the initial residual \mathbf{r}_0 onto $\text{span}\{\mathbf{S}\}$ is zero.

Proof. It holds that

$$\begin{aligned}
 \mathbf{P}_S \mathbf{r}_0 &= \mathbf{P}_S (\hat{\mathbf{y}} - \mathbf{m}) - \mathbf{P}_S \hat{\mathbf{K}} \mathbf{v}_0 \\
 &= \mathbf{P}_S (\hat{\mathbf{y}} - \mathbf{m}) - \mathbf{P}_S \hat{\mathbf{K}} \mathbf{C}_0 (\hat{\mathbf{y}} - \mathbf{m}) \\
 &= \mathbf{P}_S (\hat{\mathbf{y}} - \mathbf{m}) - \underbrace{\mathbf{S}(\mathbf{S}^\top \mathbf{S})^{-1} (\mathbf{S}^\top \hat{\mathbf{K}} \mathbf{S})}_{=\mathbf{P}_S} \underbrace{(\mathbf{S}^\top \hat{\mathbf{K}} \mathbf{S})^{-1} \mathbf{S}^\top}_{=\mathbf{C}_0} (\hat{\mathbf{y}} - \mathbf{m}) \\
 &= \mathbf{P}_S (\hat{\mathbf{y}} - \mathbf{m}) - \underbrace{\mathbf{S}(\mathbf{S}^\top \mathbf{S})^{-1} \mathbf{S}^\top}_{=\mathbf{P}_S} (\hat{\mathbf{y}} - \mathbf{m}) \\
 &= 0.
 \end{aligned}$$

□

Proposition B.3 shows that the residual in $\text{span}\{\mathbf{S}\}$ is zero. In that sense, the solution within this subspace is already perfectly identified at initialization. The remaining residual thus lies in the orthogonal complement of $\text{span}\{\mathbf{S}\}$ which can be targeted through additional actions. If we measure the error in the representer weights $\mathbf{v} - \mathbf{v}_0$, a similar results holds, as we show in the following.

Proposition B.4 (Error in Representer Weights in $\text{span}\{\mathbf{S}\}$ Is Zero)

The $\hat{\mathbf{K}}$ -orthogonal projection of the representer weights approximation error $\hat{\mathbf{P}}_S(\mathbf{v} - \mathbf{v}_0)$ onto $\text{span}\{\mathbf{S}\}$ is zero.

Proof. The $\hat{\mathbf{K}}$ -orthogonal (orthogonal with respect to the inner product $\langle \cdot, \cdot \rangle_{\hat{\mathbf{K}}}$) projection onto the subspace $\text{span}\{\mathbf{S}\}$ spanned by the actions is given by $\hat{\mathbf{P}}_S = \mathbf{C}_0 \hat{\mathbf{K}}$ (Wenger et al., 2022b, Section S2.1). It holds that

$$\begin{aligned}
 \hat{\mathbf{P}}_S(\mathbf{v} - \mathbf{v}_0) &= \mathbf{C}_0 \hat{\mathbf{K}}(\mathbf{v} - \mathbf{v}_0) \\
 &= \mathbf{C}_0 \hat{\mathbf{K}} \hat{\mathbf{K}}^{-1} (\hat{\mathbf{y}} - \mathbf{m}) - \mathbf{C}_0 \hat{\mathbf{K}} \mathbf{C}_0 \underbrace{(\hat{\mathbf{y}} - \mathbf{m})}_{=\hat{\mathbf{K}} \mathbf{v}} \\
 &= \mathbf{C}_0 (\hat{\mathbf{y}} - \mathbf{m}) - \underbrace{\mathbf{C}_0 \hat{\mathbf{K}}}_{=\hat{\mathbf{P}}_S} \underbrace{\mathbf{C}_0 \hat{\mathbf{K}}}_{=\hat{\mathbf{P}}_S} \mathbf{v} \\
 &= \mathbf{C}_0 (\hat{\mathbf{y}} - \mathbf{m}) - \mathbf{C}_0 \underbrace{\hat{\mathbf{K}} \mathbf{v}}_{=\hat{\mathbf{y}} - \mathbf{m}} \\
 &= 0,
 \end{aligned}$$

where we used that $\mathbf{v} = \hat{\mathbf{K}}^{-1}(\hat{\mathbf{y}} - \mathbf{m})$ is the solution of the GP regression linear system, $\mathbf{v}_0 = \mathbf{C}_0(\hat{\mathbf{y}} - \mathbf{m})$ and the idempotence of the projection matrix $\hat{\mathbf{P}}_S = \hat{\mathbf{P}}_S \hat{\mathbf{P}}_S$. □

Probabilistic Perspective: Equation (13) describes the effect of \mathbf{C}_0 from a probabilistic perspective. Initializing $\mathbf{C}_0 = \mathbf{0}$ in step i results in $m_{i,0} = m(\cdot)$ (prior mean) and $K_{i,0} = K(\cdot, \cdot)$ (prior covariance) since the *reduction* of uncertainty $K(\cdot, \mathbf{X}) \mathbf{C}_0 K(\mathbf{X}, \cdot)$ is zero. This case, where no information from past steps is included, is illustrated in the first column $R = 0$ in Figure 4.

Special Case: We consider a special case, where the general intricate form of the total marginal variance from Section 3.5

$$\text{Tr}(K_{i,0}(\mathbf{X}, \mathbf{X})) = \text{Tr}(\mathbf{K}) - \text{Tr}(\mathbf{K}\mathbf{C}_0\mathbf{K}) \quad (17)$$

collapses. Let $\lambda_1, \dots, \lambda_{NC} > 0$ denote the eigenvalues of $\hat{\mathbf{K}}$ and $\mathbf{b}_1, \dots, \mathbf{b}_{NC}$ the corresponding (pairwise orthogonal) eigenvectors. We make the following two assumptions: **(A1):** We assume $\mathbf{W}^{-1} = \mathbf{0}$, i.e. $\hat{\mathbf{K}} = \mathbf{K}$. **(A2):** We assume that the actions coincide with a subset $\mathbb{L} \subseteq \{1, \dots, NC\}$ of $\hat{\mathbf{K}}$'s eigenvectors $\mathbf{S} = (\mathbf{b}_l)_{l \in \mathbb{L}} \in \mathbb{R}^{NC \times |\mathbb{L}|}$.

Proposition B.5 (Total Marginal Uncertainty)
Under assumptions **(A1)** and **(A2)** it holds that

$$\text{Tr}(K_{i,0}(\mathbf{X}, \mathbf{X})) = \text{Tr}(\mathbf{K}) - \text{Tr}(\mathbf{M}).$$

Proof. Let $\mathbf{S} = (\mathbf{b}_l)_{l \in \mathbb{L}} \in \mathbb{R}^{NC \times |\mathbb{L}|}$ and $\mathbf{\Lambda} = \text{diag}((\lambda_l)_{l \in \mathbb{L}}) \in \mathbb{R}^{|\mathbb{L}| \times |\mathbb{L}|}$ contain a subset $\mathbb{L} \subseteq \{1, \dots, NC\}$ of $\hat{\mathbf{K}}$'s eigenpairs. The remaining eigenvectors and eigenvalues are given by $\mathbf{S}_+ = (\mathbf{b}_l)_{l \notin \mathbb{L}} \in \mathbb{R}^{NC \times NC - |\mathbb{L}|}$ and $\mathbf{\Lambda}_+ = \text{diag}((\lambda_l)_{l \notin \mathbb{L}}) \in \mathbb{R}^{NC - |\mathbb{L}| \times NC - |\mathbb{L}|}$. First note that we can write the eigendecomposition of $\hat{\mathbf{K}} = \mathbf{K}$ as a sum of two components $\hat{\mathbf{K}} = \mathbf{S}\mathbf{\Lambda}\mathbf{S}^\top + \mathbf{S}_+\mathbf{\Lambda}_+\mathbf{S}_+^\top$, each of which covers one part of the spectrum. It holds

$$\mathbf{S}^\top \mathbf{S} = \mathbf{I}, \quad \mathbf{S}_+^\top \mathbf{S}_+ = \mathbf{I}, \quad \mathbf{S}^\top \mathbf{S}_+ = \mathbf{0} \quad \text{and} \quad \mathbf{S}_+^\top \mathbf{S} = \mathbf{0}$$

since $\hat{\mathbf{K}}$ is symmetric and its eigenvectors are thus pairwise orthogonal. It follows

$$\begin{aligned} \mathbf{K}\mathbf{S} &= (\mathbf{S}\mathbf{\Lambda}\mathbf{S}^\top + \mathbf{S}_+\mathbf{\Lambda}_+\mathbf{S}_+^\top)\mathbf{S} = \mathbf{S}\mathbf{\Lambda} \\ \mathbf{S}^\top \mathbf{K} &= \mathbf{S}^\top (\mathbf{S}\mathbf{\Lambda}\mathbf{S}^\top + \mathbf{S}_+\mathbf{\Lambda}_+\mathbf{S}_+^\top) = \mathbf{\Lambda}\mathbf{S}^\top \\ \mathbf{M} = \mathbf{S}^\top \mathbf{K}\mathbf{S} &= \mathbf{S}^\top (\mathbf{S}\mathbf{\Lambda}\mathbf{S}^\top + \mathbf{S}_+\mathbf{\Lambda}_+\mathbf{S}_+^\top)\mathbf{S} = \mathbf{\Lambda}. \end{aligned}$$

Plugging those expressions into Equation (17) yields

$$\begin{aligned} \text{Tr}(K_{i,0}(\mathbf{X}, \mathbf{X})) &= \text{Tr}(\mathbf{K}) - \text{Tr}(\mathbf{K}\mathbf{C}_0\mathbf{K}) \\ &= \text{Tr}(\mathbf{K}) - \text{Tr}(\mathbf{K}\mathbf{S} \underbrace{(\mathbf{S}^\top \hat{\mathbf{K}} \mathbf{S})^{-1}}_{=\mathbf{M}^{-1}} \mathbf{S}^\top \mathbf{K}) \\ &= \text{Tr}(\mathbf{K}) - \text{Tr}(\mathbf{S}\mathbf{\Lambda}\mathbf{\Lambda}^{-1}\mathbf{\Lambda}\mathbf{S}^\top) \\ &= \text{Tr}(\mathbf{K}) - \text{Tr}(\mathbf{S}^\top \mathbf{S}\mathbf{\Lambda}) \\ &= \text{Tr}(\mathbf{K}) - \text{Tr}(\mathbf{\Lambda}) \\ &= \text{Tr}(\mathbf{K}) - \text{Tr}(\mathbf{M}) \\ &= \sum_{l \notin \mathbb{L}} \lambda_l. \end{aligned}$$

The last equation is due to

$$\text{Tr}(\mathbf{K}) = \text{Tr}(\mathbf{S}\mathbf{\Lambda}\mathbf{S}^\top) + \text{Tr}(\mathbf{S}_+\mathbf{\Lambda}_+\mathbf{S}_+^\top) = \text{Tr}(\mathbf{S}^\top \mathbf{S}\mathbf{\Lambda}) + \text{Tr}(\mathbf{S}_+^\top \mathbf{S}_+\mathbf{\Lambda}_+) = \text{Tr}(\mathbf{\Lambda}) + \text{Tr}(\mathbf{\Lambda}_+). \quad \square$$

Proposition B.5 shows that the *reduction* of the marginal uncertainty is determined by the sum of \mathbf{M} 's eigenvalues $\sum_{l \in \mathbb{L}} \lambda_l$. If \mathbf{S} contains the eigenvectors \mathbf{b}_l to the largest eigenvalues (i.e. \mathbf{S} is ‘‘aligned’’ with the high-variance subspace of $\hat{\mathbf{K}}$), the remaining uncertainty $\sum_{l \notin \mathbb{L}} \lambda_l$ is small. In contrast, if \mathbf{S} covers the low-variance subspace of $\hat{\mathbf{K}}$, the uncertainty remains largely unaffected.

B.4. Derivatives of the Poisson Log Likelihood

One of our main experiments in Section 5 is Poisson regression (see Appendix D.2 for details). In order to apply ITERGLM, we have to formulate the problem within the GLM framework. In particular, we have to specify the derivatives of the log likelihood.

The Poisson likelihood is given by

$$p(\mathbf{y} | \mathbf{f}) = \prod_{n=1}^N \frac{\lambda_n^{y_n} \exp(-\lambda_n)}{y_n!},$$

where $y_n \in \mathbb{N}_0$ and $\boldsymbol{\lambda} := \lambda(\mathbf{X}) = \exp(f(\mathbf{X})) = \exp(\mathbf{f})$. Taking the logarithm yields

$$\log p(\mathbf{y} | \mathbf{f}) = \sum_{n=1}^N \log \left(\frac{\lambda_n^{y_n} \exp(-\lambda_n)}{y_n!} \right) = \sum_{n=1}^N (y_n \log(\lambda_n) - \lambda_n - \log(y_n!)).$$

The log likelihood's gradient and Hessian with respect to \mathbf{f} are therefore given by

$$\nabla \log p(\mathbf{y} | \mathbf{f}) = \mathbf{y} - \exp(\mathbf{f}) \quad \text{and} \quad \nabla^2 \log p(\mathbf{y} | \mathbf{f}) = -\text{diag}(\exp(\mathbf{f})),$$

where the exponential function is applied element-wise. This implies that the log likelihood is concave which was one of the prerequisites of our algorithm (see Section 2.1). It follows that $\mathbf{W}(\mathbf{f})^{-1} = \text{diag}(\exp(-\mathbf{f}))$.

B.5. Pseudo-Inverse of Negative Hessian of the Log Likelihood for Multi-Class Classification

For multi-class classification (see Appendix D.3 for details), we need access to the pseudo inverse \mathbf{W}^\dagger . For this to be efficient, we derive an explicit form of \mathbf{W}^\dagger in the following and show that matrix-vector multiplies can be implemented efficiently in $\mathcal{O}(NC)$. Since the ordering (see Appendix C.1) of \mathbf{W} plays an important role in the derivation, we use an explicit notation in this section.

Lemma B.6 (Explicit Pseudo-Inverse for Multi-Class Classification)

Consider multi-class classification, such that the log likelihood $\log p(\mathbf{y} | \mathbf{f})$ is given by a categorical likelihood with a softmax inverse link function, then the pseudoinverse of $\mathbf{W}(\mathbf{f})$ in CN -ordering is given by

$$[\mathbf{W}(\mathbf{f})]_{CN}^\dagger = \begin{pmatrix} (\mathbf{I} - \frac{1}{C} \mathbf{1}\mathbf{1}^\top) \text{diag}(\boldsymbol{\pi}_1^{-1}) (\mathbf{I} - \frac{1}{C} \mathbf{1}\mathbf{1}^\top) & & \\ & \ddots & \\ & & (\mathbf{I} - \frac{1}{C} \mathbf{1}\mathbf{1}^\top) \text{diag}(\boldsymbol{\pi}_N^{-1}) (\mathbf{I} - \frac{1}{C} \mathbf{1}\mathbf{1}^\top) \end{pmatrix} \in \mathbb{R}^{NC \times NC},$$

where $\boldsymbol{\pi}_n = (\pi_n^1, \dots, \pi_n^C)^\top \in \mathbb{R}^C$ denotes the output of the softmax for \mathbf{x}_n , i.e. $\pi_n^c := \exp(f_n^c) / \sum_{c'} \exp(f_n^{c'})$. The cost of one matrix-vector multiplication $\mathbf{v} \mapsto [\mathbf{W}(\mathbf{f})]_{CN}^\dagger \mathbf{v}$ with the pseudo-inverse is $\mathcal{O}(NC)$.

Proof. By Eq. (3.38) in Rasmussen & Williams (2006), the matrix $\mathbf{W}(\mathbf{f})$ in NC -ordering is given by

$$[\mathbf{W}(\mathbf{f})]_{NC} = [\text{diag}(\boldsymbol{\pi})]_{NC} - \boldsymbol{\Pi}\boldsymbol{\Pi}^\top,$$

where $[\text{diag}(\boldsymbol{\pi})]_{NC} = \text{diag}(\pi_1^1, \dots, \pi_N^1, \dots, \pi_1^C, \dots, \pi_N^C)$ and

$$\boldsymbol{\Pi} = \begin{pmatrix} \text{diag}(\pi_1^1, \dots, \pi_N^1) \\ \vdots \\ \text{diag}(\pi_1^C, \dots, \pi_N^C) \end{pmatrix} \in \mathbb{R}^{NC \times N}.$$

Rewriting $\mathbf{W}(\mathbf{f})$ in the CN -ordering, we obtain using $[\text{diag}(\boldsymbol{\pi})]_{CN} = \text{diag}(\pi_1^1, \dots, \pi_1^C, \dots, \pi_N^1, \dots, \pi_N^C)$ that

$$[\mathbf{W}(\mathbf{f})]_{CN} = [\text{diag}(\boldsymbol{\pi})]_{CN} - \begin{pmatrix} \boldsymbol{\pi}_1 & & \\ & \ddots & \\ & & \boldsymbol{\pi}_N \end{pmatrix} \begin{pmatrix} \boldsymbol{\pi}_1^\top & & \\ & \ddots & \\ & & \boldsymbol{\pi}_N^\top \end{pmatrix} = \text{blockdiag}(\text{diag}(\boldsymbol{\pi}_n) - \boldsymbol{\pi}_n \boldsymbol{\pi}_n^\top).$$

Now the pseudoinverse of a block-diagonal matrix is the block-diagonal of the block pseudoinverses, i.e. $\text{blockdiag}(\mathbf{A}_n)^\dagger = \text{blockdiag}(\mathbf{A}_n^\dagger)$ which can be shown by simply checking the definition criteria of the pseudo-inverse and using basic properties of block matrices. Therefore it suffices to show that the block pseudoinverses are given by

$$(\text{diag}(\boldsymbol{\pi}_n) - \boldsymbol{\pi}_n \boldsymbol{\pi}_n^\top)^\dagger = (\mathbf{I} - \frac{1}{C} \mathbf{1}\mathbf{1}^\top) \text{diag}(\boldsymbol{\pi}_n^{-1}) (\mathbf{I} - \frac{1}{C} \mathbf{1}\mathbf{1}^\top)$$

for $n \in \{1, \dots, N\}$. We do so by checking the definition criteria of a pseudoinverse. Let $\mathbf{A}_n = \text{diag}(\boldsymbol{\pi}_n) - \boldsymbol{\pi}_n \boldsymbol{\pi}_n^\top$. We begin by showing the following intermediate result:

$$\mathbf{A}_n \left(\mathbf{I} - \frac{1}{C} \mathbf{1} \mathbf{1}^\top \right) = \mathbf{A}_n - \frac{1}{C} (\text{diag}(\boldsymbol{\pi}_n) - \boldsymbol{\pi}_n \boldsymbol{\pi}_n^\top) \mathbf{1} \mathbf{1}^\top = \mathbf{A}_n - \frac{1}{C} (\boldsymbol{\pi}_n - \boldsymbol{\pi}_n (\boldsymbol{\pi}_n^\top \mathbf{1})) \mathbf{1}^\top = \mathbf{A}_n. \quad (18)$$

Now let's verify the first criterion in the definition of the pseudoinverse. We have

$$\begin{aligned} \mathbf{A}_n \left(\mathbf{I} - \frac{1}{C} \mathbf{1} \mathbf{1}^\top \right) \text{diag}(\boldsymbol{\pi}_n^{-1}) \left(\mathbf{I} - \frac{1}{C} \mathbf{1} \mathbf{1}^\top \right) \mathbf{A}_n &= \mathbf{A}_n \text{diag}(\boldsymbol{\pi}_n^{-1}) \mathbf{A}_n \\ &= \mathbf{A}_n \text{diag}(\boldsymbol{\pi}_n^{-1}) (\text{diag}(\boldsymbol{\pi}_n) - \boldsymbol{\pi}_n \boldsymbol{\pi}_n^\top) = \mathbf{A}_n (\mathbf{I} - \mathbf{1} \boldsymbol{\pi}_n^\top) \\ &= \mathbf{A}_n - (\text{diag}(\boldsymbol{\pi}_n) - \boldsymbol{\pi}_n \boldsymbol{\pi}_n^\top) \mathbf{1} \boldsymbol{\pi}_n^\top \\ &= \mathbf{A}_n, \end{aligned}$$

where we used (18). Next, we'll verify the second criterion.

$$\begin{aligned} \left(\mathbf{I} - \frac{1}{C} \mathbf{1} \mathbf{1}^\top \right) \text{diag}(\boldsymbol{\pi}_n^{-1}) \left(\mathbf{I} - \frac{1}{C} \mathbf{1} \mathbf{1}^\top \right) \mathbf{A}_n \left(\mathbf{I} - \frac{1}{C} \mathbf{1} \mathbf{1}^\top \right) \text{diag}(\boldsymbol{\pi}_n^{-1}) \left(\mathbf{I} - \frac{1}{C} \mathbf{1} \mathbf{1}^\top \right) \\ = \left(\mathbf{I} - \frac{1}{C} \mathbf{1} \mathbf{1}^\top \right) \text{diag}(\boldsymbol{\pi}_n^{-1}) \mathbf{A}_n \text{diag}(\boldsymbol{\pi}_n^{-1}) \left(\mathbf{I} - \frac{1}{C} \mathbf{1} \mathbf{1}^\top \right) \\ = \left(\mathbf{I} - \frac{1}{C} \mathbf{1} \mathbf{1}^\top \right) (\boldsymbol{\pi}_n^{-1}) \left(\mathbf{I} - \frac{1}{C} \mathbf{1} \mathbf{1}^\top \right) \end{aligned}$$

where we used

$$\text{diag}(\boldsymbol{\pi}_n^{-1}) \mathbf{A}_n = \mathbf{I} = \mathbf{A}_n \text{diag}(\boldsymbol{\pi}_n^{-1}) \quad (19)$$

as shown above. Finally, we verify the symmetry of the product of \mathbf{A}_n and its pseudoinverse. Observe that both \mathbf{A}_n and $\left(\mathbf{I} - \frac{1}{C} \mathbf{1} \mathbf{1}^\top \right) \text{diag}(\boldsymbol{\pi}_n^{-1}) \left(\mathbf{I} - \frac{1}{C} \mathbf{1} \mathbf{1}^\top \right)$ are symmetric. Therefore we have

$$\left(\mathbf{A}_n \left(\mathbf{I} - \frac{1}{C} \mathbf{1} \mathbf{1}^\top \right) \text{diag}(\boldsymbol{\pi}_n^{-1}) \left(\mathbf{I} - \frac{1}{C} \mathbf{1} \mathbf{1}^\top \right) \right)^* = \left(\mathbf{I} - \frac{1}{C} \mathbf{1} \mathbf{1}^\top \right) \text{diag}(\boldsymbol{\pi}_n^{-1}) \left(\mathbf{I} - \frac{1}{C} \mathbf{1} \mathbf{1}^\top \right) \mathbf{A}_n$$

and

$$\left(\left(\mathbf{I} - \frac{1}{C} \mathbf{1} \mathbf{1}^\top \right) \text{diag}(\boldsymbol{\pi}_n^{-1}) \left(\mathbf{I} - \frac{1}{C} \mathbf{1} \mathbf{1}^\top \right) \mathbf{A}_n \right)^* = \mathbf{A}_n \left(\mathbf{I} - \frac{1}{C} \mathbf{1} \mathbf{1}^\top \right) \text{diag}(\boldsymbol{\pi}_n^{-1}) \left(\mathbf{I} - \frac{1}{C} \mathbf{1} \mathbf{1}^\top \right).$$

Thus if we can show that \mathbf{A}_n and $\left(\mathbf{I} - \frac{1}{C} \mathbf{1} \mathbf{1}^\top \right) \text{diag}(\boldsymbol{\pi}_n^{-1}) \left(\mathbf{I} - \frac{1}{C} \mathbf{1} \mathbf{1}^\top \right)$ commute we have shown the remaining symmetry criteria of the pseudoinverse. It holds that

$$\mathbf{A}_n \left(\mathbf{I} - \frac{1}{C} \mathbf{1} \mathbf{1}^\top \right) \text{diag}(\boldsymbol{\pi}_n^{-1}) \left(\mathbf{I} - \frac{1}{C} \mathbf{1} \mathbf{1}^\top \right) \stackrel{(18)}{=} \mathbf{A}_n \text{diag}(\boldsymbol{\pi}_n^{-1}) \left(\mathbf{I} - \frac{1}{C} \mathbf{1} \mathbf{1}^\top \right) \stackrel{(19)}{=} \left(\mathbf{I} - \frac{1}{C} \mathbf{1} \mathbf{1}^\top \right)$$

as well as

$$\left(\mathbf{I} - \frac{1}{C} \mathbf{1} \mathbf{1}^\top \right) \text{diag}(\boldsymbol{\pi}_n^{-1}) \left(\mathbf{I} - \frac{1}{C} \mathbf{1} \mathbf{1}^\top \right) \mathbf{A}_n \stackrel{(18)}{=} \left(\mathbf{I} - \frac{1}{C} \mathbf{1} \mathbf{1}^\top \right) \text{diag}(\boldsymbol{\pi}_n^{-1}) \mathbf{A}_n \stackrel{(19)}{=} \left(\mathbf{I} - \frac{1}{C} \mathbf{1} \mathbf{1}^\top \right)$$

This completes the proof for the form of the pseudoinverse. For the complexity of multiplication, note that multiplying with $\left(\mathbf{I} - \frac{1}{C} \mathbf{1} \mathbf{1}^\top \right) \text{diag}(\boldsymbol{\pi}_n^{-1}) \left(\mathbf{I} - \frac{1}{C} \mathbf{1} \mathbf{1}^\top \right)$ has cost $\mathcal{O}(C)$, since it decomposes into two multiplications with $\left(\mathbf{I} - \frac{1}{C} \mathbf{1} \mathbf{1}^\top \right)$ which is linear and one elementwise scaling. Therefore the cost of multiplication with the pseudoinverse consisting of N blocks has complexity $\mathcal{O}(NC)$. \square

C. Implementation Details

C.1. Ordering within Vectors & Matrices

Ordering within Vectors: By default, we assume all vectors and matrices to be represented in CN -ordering. For example, the mean vector was introduced as the aggregated outputs of the mean function $m: \mathbb{X} \rightarrow \mathbb{R}^C$ for all data points $\mathbf{m} = m(\mathbf{X}) = (m(\mathbf{x}_1)^\top, \dots, m(\mathbf{x}_N)^\top)^\top$. With $m(\mathbf{x}_n)^\top = (m_n^1, \dots, m_n^C)$ denoting the C outputs for data point \mathbf{x}_n , we

can write \mathbf{m} as $\mathbf{m} = (m_1^1, m_1^2, \dots, m_1^C, \dots, m_N^1, m_N^2, \dots, m_N^C)$. We call that representation *CN*-ordering because the superscript c moves *first* and the subscript n moves *second*. Consecutively, $(m_1^1, m_2^1, \dots, m_N^1, \dots, m_1^C, m_2^C, \dots, m_N^C)$ corresponds to *NC*-ordering.

Ordering within Matrices: The same terminology can be applied to matrices, where the rows and columns can be represented in *CN* or *NC*-ordering. Depending on the context, different representations are beneficial. For example, in *CN*-ordering, \mathbf{W} is block-diagonal (due to our iid assumption, see Section 2.1) with N blocks of size $C \times C$ on the diagonal. In contrast, when the C outputs of the hidden function are assumed to be independent of each other, \mathbf{K} is block diagonal only in *NC*-ordering. So, based on the chosen ordering, different structures arise that we can exploit in subsequent computations (e.g. when we compute the inverse of \mathbf{W} , see Appendix C.4).

C.2. ITERGLM Outer Loop

Our algorithm ITERGLM approximates the posterior mode through a sequence of (approximate) Newton steps. Algorithm 2 describes this outer loop.

Algorithm 2: ITERGLM Outer loop.

Input: GP prior $\mathcal{GP}(m, K)$, training data (\mathbf{X}, \mathbf{y}) , $\nabla p(\mathbf{y}|\mathbf{f}, \mathbf{X})$ and access to products with \mathbf{K} and $\mathbf{W}(\mathbf{f})^{-1}$

Output: GP posterior $\mathcal{GP}(m_{i,j}, K_{i,j})$

1	procedure ITERGLM($m, K, \mathbf{X}, \mathbf{y}, \mathbf{f}_0 = \mathbf{m}$)		
2	$\mathbf{m} \leftarrow m(\mathbf{X})$,	Prior mean vector	$\mathcal{O}(\tau_m)$
3	Provide access to $\mathbf{w} \mapsto \mathbf{K}\mathbf{w}$	Prior covariance/kernel matrix	$\mathcal{O}(\mu_K)$
4	Initialize buffers $\mathbf{S}, \mathbf{T} \in \mathbb{R}^{NC \times 0}$	Buffers for actions and products with \mathbf{K}	
5	for $i = 0, 1, 2, \dots$ while not STOPPINGCRITERION() do		
6	Provide access to $\mathbf{w} \mapsto \mathbf{W}(\mathbf{f}_i)^{-1}\mathbf{w}$	Observation noise	$\mathcal{O}(\mu_{W^{-1}})$
7	$\hat{\mathbf{y}}(\mathbf{f}_i) \leftarrow \mathbf{f}_i + \mathbf{W}(\mathbf{f}_i)^{-1}\nabla \log p(\mathbf{y} \mathbf{f}_i, \mathbf{X})$	Pseudo regression targets	$\mathcal{O}(\tau_{W^{-1}} + NC)$
8	$m_{i,j}, K_{i,j} \leftarrow \text{ITERGP}(m, K, \mathbf{X}, \mathbf{y}, \mathbf{m}, \mathbf{K}, \mathbf{W}(\mathbf{f}_i)^{-1}, \hat{\mathbf{y}}(\mathbf{f}_i), \mathbf{S}, \mathbf{T})$	Algorithm 3	$\mathcal{O}(NC)$
9	$\mathbf{f}_{i+1} \leftarrow \mathbf{K}\mathbf{v} + \mathbf{m}$	Approximate Newton update	$\mathcal{O}(\tau_K + NC)$
10	return $\mathcal{GP}(m_{i,j}, K_{i,j})$		

Instructions in blue are needed for recycling (see Section 3.4). The matrices \mathbf{K} and $\mathbf{W}^{-1}(\mathbf{f}_i)$ are evaluated lazily. We thus report the runtime costs when the matrix-vector products are actually computed. For an in-depth discussion of the computational costs, see Appendix C.4.

The STOPPINGCRITERION() we use for our experiments is based on the *relative change* of the vector $\mathbf{g}_i = \mathbf{f}_i - \mathbf{m}$. When $\|\mathbf{g}_i - \mathbf{g}_{i-1}\| \|\mathbf{g}_i\|^{-1} \leq \delta$ falls below the convergence tolerance δ (by default, $\delta = 1\%$), the loop over i terminates. Of course, other convergence criteria are also conceivable. Depending on the application one might want to customize the criterion and, for example, include the marginal uncertainty at the training data.

C.3. ITERGLM Inner Loop: ITERGP with a Virtual Solver Run

The core of ITERGLM is ITERGP (Wenger et al., 2022b): ITERGP is used to approximate the Newton updates defined in the outer loop. Our version of the algorithm, given in Algorithm 3, adds a virtual solver run (see Algorithm 1) for efficient recycling between outer loop steps.

We use the same STOPPINGCRITERION() as in (Wenger et al., 2022b, Section S3.2): The loop over j terminates if the norm of the residual $\|\mathbf{r}_j\| < \max\{\delta_{\text{abs}}, \delta_{\text{rel}}\|\hat{\mathbf{y}} - \mathbf{m}\|\}$ is below an absolute tolerance δ_{abs} or below the scaled norm of the right-hand side $\hat{\mathbf{y}} - \mathbf{m}$ of the linear system. By default, both tolerances are set to 10^{-5} . Additionally, we typically specify a maximum number of iterations. The solver is also terminated when the normalization constant $\eta_j \leq 0$. This can happen due to numerical imprecision if the linear system is badly conditioned, e.g. if some eigenvalues of the linear system are close to zero.

C.4. Cost Analysis of ITERGLM

In this section, we investigate the computational costs of ITERGLM in more detail. We start with a discussion of the computational costs for matrix-vector products with \mathbf{K} , \mathbf{W}^{-1} and C_j and then analyze the runtime and memory costs of the individual algorithms (Algorithms 1, 2 and 3).

Algorithm 3: ITERGLM Inner Loop: ITERGP with a Virtual Solver Run.
Input: GP prior $\mathcal{GP}(m, K)$, training data (\mathbf{X}, \mathbf{y}) , m , products with K and \mathbf{W}^{-1} , pseudo targets $\hat{\mathbf{y}}$, buffers \mathbf{S}, \mathbf{T}
Output: GP posterior $\mathcal{GP}(m_{i,j}, K_{i,j})$

		Time	Memory
1	procedure ITERGP($m, K, \mathbf{X}, \mathbf{y}, m, \mathbf{K}, \mathbf{W}^{-1}, \hat{\mathbf{y}}(f_i), \mathbf{S}, \mathbf{T}$)		
2	$\mathbf{C}_0, \mathbf{S}, \mathbf{T} \leftarrow \text{VIRTUALSOLVERRUN}(\mathbf{S}, \mathbf{T}, \mathbf{W}^{-1})$	Algorithm 1, $\mathbf{C}_0 = \mathbf{Q}_0 \mathbf{Q}_0^\top$	
3	$\mathbf{v}_0 \leftarrow \mathbf{C}_0(\hat{\mathbf{y}} - m)$	Consistent initial iterate	$\mathcal{O}(N C)$
4	for $j = 1, 2, 3, \dots$ while not STOPPINGCRITERION() do		
5	$\mathbf{r}_{j-1} \leftarrow (\hat{\mathbf{y}} - m) - \mathbf{K} \mathbf{v}_{j-1} - \mathbf{W}^{-1} \mathbf{v}_{j-1}$	Predictive residual	$\mathcal{O}(\tau_K + \tau_{\mathbf{W}^{-1}} + N C)$
6	$\mathbf{s}_j \leftarrow \text{POLICY}()$	Select action via policy	$\mathcal{O}(\tau_{\text{POLICY}})$
7	Append \mathbf{s}_j to buffer $\mathbf{S} \leftarrow (\mathbf{S}, \mathbf{s}_j) \in \mathbb{R}^{N C \times B}$	B : current buffer size	$\mathcal{O}(B N C)$
8	$\alpha_j \leftarrow \mathbf{s}_j^\top \mathbf{r}_{j-1}$	Observation via information operator	$\mathcal{O}(N C)$
9	$\mathbf{t}_j \leftarrow \mathbf{K} \mathbf{s}_j$	First component of $\hat{\mathbf{K}} \mathbf{s}_j = \mathbf{K} \mathbf{s}_j + \mathbf{W}^{-1} \mathbf{s}_j$	$\mathcal{O}(\tau_K)$
10	Append \mathbf{t}_j to buffer $\mathbf{T} \leftarrow (\mathbf{T}, \mathbf{t}_j) \in \mathbb{R}^{N C \times B}$	B : current buffer size	$\mathcal{O}(B N C)$
11	$\mathbf{z}_j \leftarrow \mathbf{t}_j + \mathbf{W}^{-1} \mathbf{s}_j$	Add second component of $\hat{\mathbf{K}} \mathbf{s}_j = \mathbf{K} \mathbf{s}_j + \mathbf{W}^{-1} \mathbf{s}_j$	$\mathcal{O}(\tau_{\mathbf{W}^{-1}} + N C)$
12	$\mathbf{d}_j \leftarrow \mathbf{s}_j - \mathbf{C}_{j-1} \mathbf{z}_j$	Search direction	$\mathcal{O}(B N C)$
13	$\eta_j \leftarrow \mathbf{z}_j^\top \mathbf{d}_j$	Normalization constant	$\mathcal{O}(N C)$
14	$\mathbf{Q}_j \leftarrow (\mathbf{Q}_{j-1}, \frac{1}{\sqrt{\eta_j}} \mathbf{d}_j) \in \mathbb{R}^{N C \times B}$	Append column to matrix root	$\mathcal{O}(N C)$
15	$\mathbf{C}_j \leftarrow \mathbf{Q}_j \mathbf{Q}_j^\top$	Rank B approximation $\mathbf{C}_j = \mathbf{C}_{j-1} + \frac{1}{\eta_j} \mathbf{d}_j \mathbf{d}_j^\top \approx \hat{\mathbf{K}}^{-1}$	
16	$\mathbf{v}_j \leftarrow \mathbf{v}_{j-1} + \frac{\alpha_j}{\eta_j} \mathbf{d}_j$	Representer weights (i.e. solution) estimate	$\mathcal{O}(N C)$
17	$m_{i,j}(\cdot) \leftarrow m(\cdot) + K(\cdot, \mathbf{X}) \mathbf{v}_j$	Approximate posterior mean, Eq. (12)	$\mathcal{O}(N N_\diamond C^2)$
18	$K_{i,j}(\cdot, \cdot) \leftarrow K(\cdot, \cdot) - K(\cdot, \mathbf{X}) \mathbf{C}_j K(\mathbf{X}, \cdot)$	Covariance function, Eq. (13)	$\mathcal{O}(B(N + N_\diamond) N_\diamond C^2)$
19	return $\mathcal{GP}(m_{i,j}, K_{i,j})$		

Instructions in blue are needed for recycling (see Section 3.4). \mathbf{C}_j is represented via its root \mathbf{Q}_j and evaluated lazily. We thus report the runtime costs when the matrix-vector products are actually computed. The costs for evaluating the posterior GP $\mathcal{GP}(m_{i,j}, K_{i,j})$ are based on N_\diamond test data points $\mathbf{X}_\diamond \in \mathbb{R}^{N_\diamond \times D}$. For an in-depth discussion of the computational costs, see Appendix C.4.

C.4.1. MATRIX-VECTOR PRODUCTS

ITERGP is an *iterative matrix-free* algorithm and our algorithm ITERGLM inherits that property: The matrices \mathbf{K} , \mathbf{W}^{-1} and \mathbf{C}_j are evaluated lazily, i.e. matrix-vector products are evaluated *without* forming the matrices in memory explicitly. This enables our algorithm to scale to problems where a naive approach causes memory overflows. In Algorithms 1, 2 and 3, the memory and runtime cost for matrix-vector products with \mathbf{K} are denoted by μ_K and τ_K and by $\mu_{\mathbf{W}^{-1}}$ and $\tau_{\mathbf{W}^{-1}}$ for products with \mathbf{W}^{-1} .

Products with \mathbf{K} : Matrix-vector products with \mathbf{K} can be decomposed into products with its sub-matrices. The associated memory costs $\mathcal{O}(\mu_K)$ can thereby be reduced basically arbitrarily and the runtime can be improved by using specialized software libraries such as KEOPS (Charlier et al., 2021) and parallel hardware (i.e. GPUs). Still, products with \mathbf{K} are computationally relatively expensive, since this operation is typically *quadratic* in the number of training data points N .

Products with \mathbf{W}^{-1} (General Case): Under the assumptions on the likelihood from Section 2.1, \mathbf{W} is block-diagonal with N blocks of size $C \times C$ (in CN -ordering, see Appendix C.1). Here, we denote these blocks by $\mathbf{W}_1, \dots, \mathbf{W}_N$. It can be easily verified that \mathbf{W}^{-1} is also a block-diagonal matrix and the blocks on its diagonal are the inverses of $\mathbf{W}_1, \dots, \mathbf{W}_N$.

Consider the matrix-vector product $\mathbf{v} \mapsto \mathbf{W}^{-1} \mathbf{v} =: \mathbf{w} \in \mathbb{R}^{N C}$. In the vectors \mathbf{v} and \mathbf{w} , we repeatedly group C consecutive entries which results in segments $\mathbf{w}_n, \mathbf{v}_n \in \mathbb{R}^C$ for $n = 1, \dots, N$, i.e.

$$\underbrace{\begin{pmatrix} \mathbf{W}_1^{-1} & & \\ & \ddots & \\ & & \mathbf{W}_N^{-1} \end{pmatrix}}_{=\mathbf{W}^{-1}} \cdot \underbrace{\begin{pmatrix} \mathbf{v}_1 \\ \vdots \\ \mathbf{v}_N \end{pmatrix}}_{=\mathbf{v}} = \underbrace{\begin{pmatrix} \mathbf{w}_1 \\ \vdots \\ \mathbf{w}_N \end{pmatrix}}_{=\mathbf{w}}.$$

It holds that $\mathbf{w}_n = \mathbf{W}_n^{-1} \mathbf{v}_n$, i.e. each segment in \mathbf{w} is the product of a single $C \times C$ block from \mathbf{W}^{-1} with one segment from \mathbf{v} . Computing \mathbf{w}_n thus amounts to solving a linear system of size C with cost $\mathcal{O}(C^3)$. The total cost for all N segments is thus $\mathcal{O}(N C^3)$. However, the N linear systems are independent of each other and can thus be solved in parallel. So, if

appropriate computational resources are available, the total runtime complexity can be reduced to $\mathcal{O}(C^3)$.

In general, \mathbf{W}^{-1} requires $\mathcal{O}(NC^2)$ in terms of memory consumption. If needed, these costs can be reduced further to $\mathcal{O}(C^2)$ because (as explained above), products with \mathbf{W}^{-1} can be broken down into products with the individual blocks of \mathbf{W}^{-1} . We can perform those products sequentially such that only a single block is present in memory at a time.

Products with \mathbf{W}^{-1} (Special Cases): In many cases, we can multiply with \mathbf{W}^{-1} more efficiently. In the multi-class classification case, the runtime and memory costs for multiplication with the pseudo inverse \mathbf{W}^\dagger can be reduced to $\mathcal{O}(NC)$ (see Appendix B.5). In the regression case ($C = 1$), \mathbf{W}^{-1} is a diagonal matrix of size $N \times N$. The memory and runtime costs are thus in $\mathcal{O}(N)$. An example is Poisson regression, for which we derive the explicit form of \mathbf{W}^{-1} in Appendix B.4.

Products with C_j : $C_j = \mathbf{Q}_j \mathbf{Q}_j^\top$ is represented via its matrix root $\mathbf{Q}_j \in \mathbb{R}^{NC \times B}$. This allows for efficient storage and matrix-vector multiplies $v \mapsto C_j v = \mathbf{Q}_j (\mathbf{Q}_j^\top v)$ in $\mathcal{O}(BNC)$.

C.4.2. COST ANALYSIS ALGORITHMS 1, 2 AND 3

The runtime and memory complexity for the operations in Algorithms 1, 2 and 3 is given directly in the pseudo code. Here, we provide some additional information for the costs that depend on the user’s choices and put the costs of the individual algorithms into perspective.

Algorithm 3 (ITERGP): The runtime cost for selecting an action $\mathcal{O}(\tau_{\text{POLICY}})$ depends on the underlying policy. For Cholesky actions ($s_j = e_j$) or CG ($s_j = r_{j-1}$), the runtime cost is insignificant since no additional computations are required at all.

One iteration’s total computational cost (without prediction) is dominated by two matrix-vector products with \mathbf{K} in terms of runtime and $\mathcal{O}(BNC)$ in terms of storage requirements (for the buffers \mathbf{S} and \mathbf{T} as well as the matrix root \mathbf{Q}_j). The *initial* size (i.e. the number of columns) of \mathbf{S} , \mathbf{T} and \mathbf{Q}_j is given by the rank limit R used in Algorithm 1. Henceforth, one column is added to each of the buffers and matrix root in *each* solver iteration, increasing their size to $B = R + j$ in iteration j . It is thus reasonable to include an upper bound on the iteration number in the stopping criterion of Algorithm 3.

Algorithm 1 (Virtual Solver Run with Optional Compression): The total runtime complexity of Algorithm 1 is $\mathcal{O}(B\tau_{\mathbf{W}^{-1}} + B^2NC)$, i.e. dominated by matrix-matrix products involving the buffers and \mathbf{W}^{-1} . In terms of memory requirements, the buffers \mathbf{S} , \mathbf{T} , and \mathbf{Q}_0 are the decisive contributors with $\mathcal{O}(RNC)$. The truncation of the eigendecomposition provides a way to control that bound by resetting the current buffer size B to an arbitrary number $R \leq B$. In comparison to Algorithm 3, the computational costs are practically of minor importance since no multiplications with \mathbf{K} are necessary.

Algorithm 2 (ITERGLM Outer Loop): The costs $\mathcal{O}(\tau_m)$ for evaluating m on the training data depends on the choice of mean function. For a constant mean function, no computations are necessary, so runtime costs are negligible. This can be different e.g. for applications in Bayesian deep learning, where evaluating m requires forward passes through a neural network.

D. Experimental Details

Throughout the paper, we use binary classification as an illustrative and supporting example (Figures 1 to 4). The two main experiments follow in Section 5: Poisson regression (Section 5.1, Figure 5) and large-scale GP multi-class classification (Section 5.2, Figure 6). In the following, we provide additional details for all those experiments.

D.1. Binary Classification

Binary Classification with *one* latent function: Consider a binary classification task, i.e. $C = 2$. Being able to report the probability for *one* of the two classes is sufficient because they have to add up to one for every data point. Thus, while $C = 2$, N -dimensional vectors are typically used to describe this problem (Rasmussen & Williams, 2006, Section 3.4). Using only a single latent function is convenient for illustrative purposes, as e.g. the action vectors \mathbf{s} in Algorithm 3 are N -dimensional (not $2N$ -dimensional) and thus easier to visualize.

1D Data: We use a one-dimensional training set in Figure 2. \mathbf{X} is created by sampling $N = 50$ data points between -3 and 5 . The hidden function f is a draw from a GP with mean zero and a GPYTORCH (Gardner et al., 2018) RBF kernel with `lengthscale = 1.0` and `outputscale = 5.0`. For each datapoint \mathbf{x}_n , we sample the positive label with probability $\text{logistic}(f(\mathbf{x}_n))$.

2D Data: Two-dimensional data is used in Figures 1, 3 and 4. The data-generating process is analogous to the 1D data, only now, the $N = 100$ training inputs are in the 2D plane: The first coordinate is sampled uniformly between -3 and 5 , the second between -4 and 1 . The hyperparameters of the RBF kernel are $\text{lengthscale} = 1.0$, $\text{outputscale} = 10.0$ for Figures 3 and 4 and $\text{outputscale} = 20.0$ for Figure 1.

Details Figure 1: In this figure, we compare two versions of our algorithm: ITERGLM-Chol without recycling and ITERGLM-CG with recycling and with compression ($R = 10$). Both runs were conducted on a CPU. The computation of the NLL loss is *not* included in the runtime measurement. A description of how the NLL loss can be computed for arbitrary C is given in Appendix D.3.

Details Figure 2: For Figure 2, we compute a sequence of *precise* Newton steps by using ITERGLM with unit vector actions and $j \leq N$ solver iterations. Note that the Newton linear system is N -dimensional, i.e. we actually obtain f_i as defined by Equation (5).

Details Figure 3: In this plot, we compare unit vector actions (ITERGLM-Chol) and residual actions (ITERGLM-CG) for the first Newton step ($i = 0$) at three solver iterations $j \in \{1, 10, 19\}$. The true posterior mean function $m_{0,*}$ and covariance function $K_{0,*}$ are computed by using ITERGLM-Chol and $j \leq N = 100$ iterations. Figure 7 shows the covariance functions corresponding to the mean functions in Figure 3.

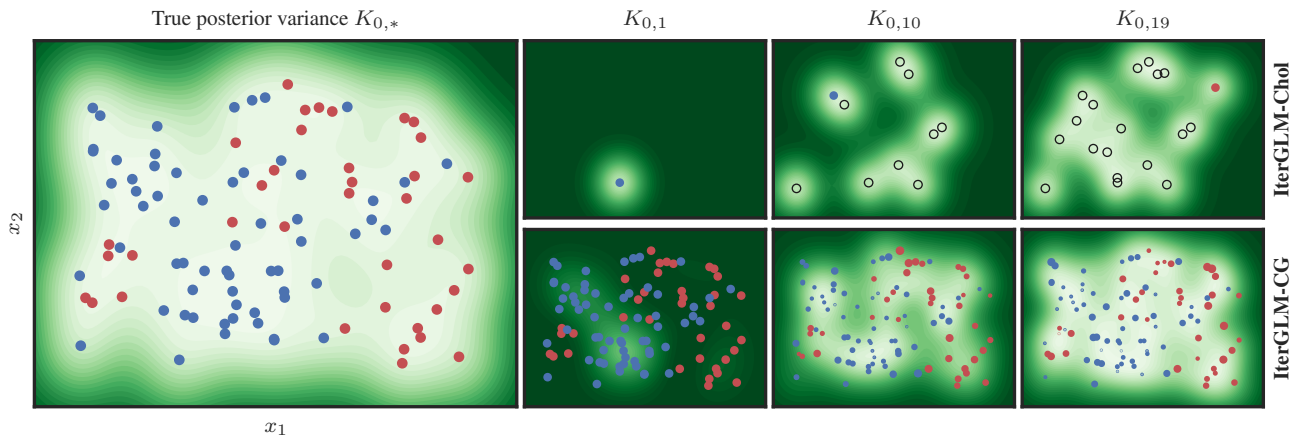


Figure 7: Different Policies of ITERGLM Applied to GP Classification. (Left) The true posterior covariance $K_{0,*}$ (■) for a binary classification task (●/●). (Right) Current estimate of the posterior covariance after 1, 10, and 19 iterations with the unit vector policy (Top) and the CG policy (Bottom). Shown are the data points selected by the policy in this iteration with the dot size indicating their relative weight. For ITERGLM-Chol, data points are targeted one by one and previously used data points are marked with (○).

The actions are visualized by scaling the training data points according to their *relative weight*: First, we take the absolute value of the action vector s from Algorithm 3 (element-wise) and then scale its entries linearly such that the smallest entry is 0 and the largest is 1.

Details Figure 4: In this figure, we show the initial mean function $m_{1,0}$ and covariance function $K_{1,0}$ in the *second* Newton step for different buffer sizes $R \in \{0, 1, 3, 10\}$. We use CG actions for the first Newton step and let the solver run until convergence (this takes 19 iterations).

D.2. Poisson Regression

In Section 5.1, we apply ITERGLM to Poisson regression to demonstrate our algorithm’s ability to generalize to other (log-concave) likelihoods and to explore the trade-off between the number of (outer loop) mode-finding steps and (inner loop) solver iterations.

Poisson Likelihood: We consider count data $y \in \mathbb{N}_0^N$ that is assumed to be generated from a Poisson likelihood with unknown positive rate $\lambda: \mathbb{X} \rightarrow \mathbb{R}_+$. Modeling λ with a GP which may take positive *and negative* values, would therefore be inappropriate. However, we can use a GP for the log rate $f: \mathbb{X} \rightarrow \mathbb{R}$ and regard this as the unknown latent function. With

$\lambda := \lambda(\mathbf{X}) = \exp(f(\mathbf{X})) = \exp(\mathbf{f})$, the likelihood is given by

$$p(\mathbf{y} | \mathbf{f}) = \prod_{n=1}^N \frac{\lambda_n^{y_n} \exp(-\lambda_n)}{y_n!}.$$

The gradient and (inverse) Hessian of the log likelihood can be derived in closed form, see [Appendix B.4](#).

Data & Model: First, we create \mathbf{X} by linearly spacing $N = 100$ points between 0 and 1. For the count data \mathbf{y} , we sample from a GP with zero mean and a GPYTORCH ([Gardner et al., 2018](#)) RBF-kernel with `lengthscale = 0.1` and `outputscale = 5.0`. That GP f represents the log Poisson rate. We then draw counts from a Poisson distribution with rate $\lambda(\mathbf{x}_n) = \exp(f(\mathbf{x}_n))$ for each data point in the training set. In this experiment, we conduct multiple ITERGLM runs on different training sets. These sets are created by re-drawing from the Poisson distributions with the same rates, i.e. the underlying GP for the log rate does *not* change. Our GLM’s prior uses the same RBF kernel to avoid model mismatch.

ITERGLM-CG Approaches: We consider ITERGLM-CG with four different schedules: A fixed budget of 100 iterations is distributed uniformly over 5, 10, 20 or 100 outer loop steps (see [Algorithm 2](#)), which limits the number of inner loop iterations (see [Algorithm 3](#)) to $j \leq 20, 10, 5$ or 1. For each schedule, we perform 10 runs with different training sets, see above. Each run uses recycling without compression. For this experiment, the convergence tolerance in [Algorithm 2](#) is set to $\delta = 0.001$.

Tracking of Performance Metrics: As a performance metric, we use the NLL loss. The computation of the NLL loss for the test and training set is *not* included in the runtime reported in the results. For the NLL loss, we approximate the integral from [Section 2.3](#) with MC samples: For each test datum \mathbf{x}_\diamond , we draw 10^5 MC samples from $\mathcal{N}(m_{i,j}(\mathbf{x}_\diamond), K_{i,j}(\mathbf{x}_\diamond, \mathbf{x}_\diamond))$, map those samples $\{f_{\diamond,k}\}_{k=1}^{10^5}$ through the likelihood $p(y_\diamond | f_{\diamond,k})$ and average. This yields a loss value for \mathbf{x}_\diamond and we obtain the training/test NLL loss by averaging these loss values for all data points in the training/test set.

Approximate Rate Distribution: Using ITERGLM-CG for the Poisson regression problem results in a sequence of posteriors $\mathcal{GP}(m_{i,j}, k_{i,j})$. By drawing MC samples from those posterior GPs and mapping them through the exponential, we obtain an approximated (skewed) distribution for the rate λ . In [Figure 5 \(Right\)](#), we report its median and a 95 % confidence interval between the 2.5 % and 97.5 % percentile.

D.3. Large-Scale GP Multi-Class Classification

In this experiment, we empirically evaluate ITERGLM on a large-scale GP multi-class classification problem to exhibit its scalability. We also investigate the impact of compression on performance.

Data: We consider a Gaussian mixture problem with $C = 10$ classes in 3D. For each class, we sample a mean vector uniformly in $[-1, 1]^3$ and a positive definite covariance matrix. For the covariance matrix, we first create a 3×3 matrix C with entries between 0 and 1 (sampled uniformly) and compute the eigenvectors U of CC^\top . Then, we create three eigenvalues $\{\lambda_d\}_{d \in \{1,2,3\}}$ uniformly between 0.001 and 0.1 and form the covariance matrix from the eigenvectors U and these eigenvalues, i.e. $U \text{diag}(\lambda_1, \lambda_2, \lambda_3) U^\top$. For each class, 10^4 data points are sampled from the respective Gaussian distribution. This amounts to $N = 10^5$ data points in total. For testing, $N_\diamond = 10^4$ data points are used (10^3 per class). Both training and test set are shown in [Figure 8](#).

Model: We use a softmax likelihood (see [Appendix B.5](#) for the details on the pseudo inverse W^\dagger) and assume independent GPs for the C outputs of the latent function. Each of these GPs uses the zero function as the prior mean and a Matérn($\frac{3}{2}$) kernel. We use the KEOPS ([Charlier et al., 2021](#)) version of the GPYTORCH ([Gardner et al., 2018](#)) kernel with `lengthscale = 0.05` and `outputscale = 0.05`.

SoD Approaches: For the SoD approaches, we create a random subset of the training data (sampling without replacement) of a specific subset size N_{sub} . We then explicitly form $\hat{K}(\mathbf{f}_i)$ for every Newton step and compute its Cholesky decomposition via PYTORCH’s ([Paszke et al., 2019](#)) `torch.linalg.cholesky` (instead of using ITERGP in [Algorithm 2](#) to ensure a competitive baseline implementation). In our experiment, we use four different subset sizes $N_{\text{sub}} \in \{250, 500, 1000, 2000\}$.

SVGP: SVGP ([Titsias, 2009](#); [Hensman et al., 2015](#)) is a commonly used variational method for approximative inference in non-conjugate GPs. We use GPYTORCH’s ([Gardner et al., 2018](#)) SVGP implementation and optimize the ELBO for 10^4 seconds using ADAM with batch size = 1024. The learning rate $\alpha \in \{0.001, 0.01, 0.05\}$ and the number of inducing points $U \in \{1000, 2500, 5000, 10000\}$ are tuned via grid search. We use U/C inducing points per class ($C = 10$ classes) and

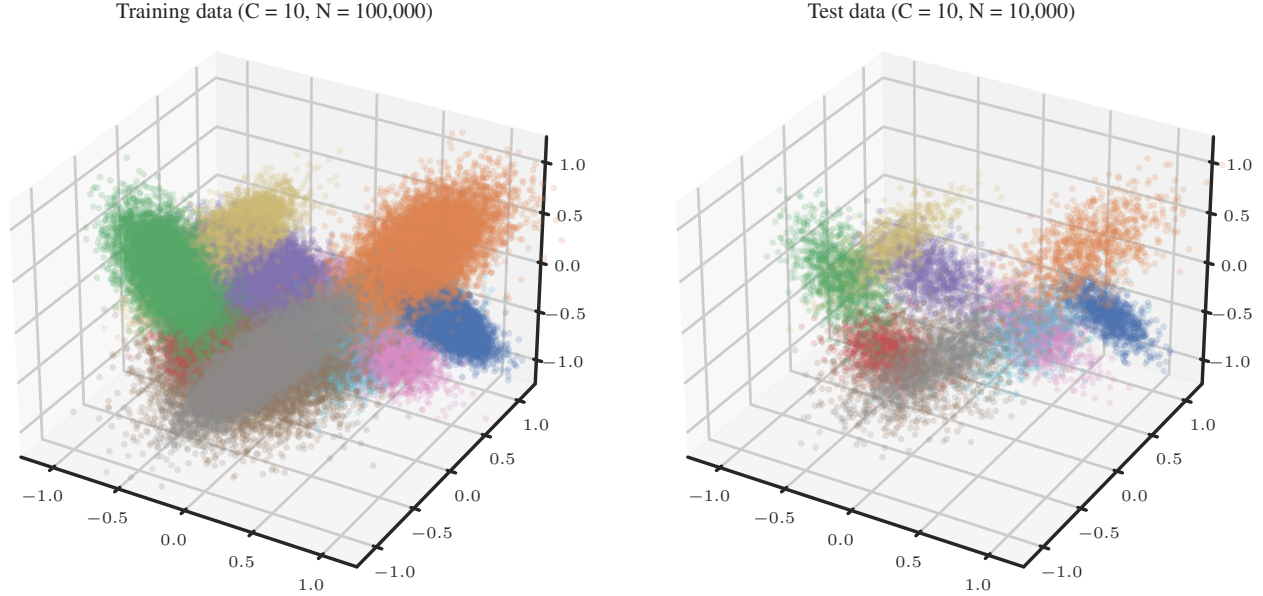


Figure 8: Gaussian Mixture Training and Test Data. (Left) Training data. (Right) Test data. Note that both sets use the same underlying Gaussians.

initialize them as a random subset of the training data. Within the given runtime budget, SVGP performs between 6000 ($U = 1000$) and 600 ($U = 10000$) epochs.

For each of the 12 runs, we extract 6 performance indicators: lowest training/test NLL loss during training, highest training/test accuracy during training and training/test expected calibration error (ECE) at the very end of training. For each of those 6 categories, we determine those three runs with the best performance. This procedure results in a set of 4 runs in total, that are considered the “best” runs for SVGP. Only those 4 (out of 12) are shown in Figure 6.

ITERGLM-CG Approaches: For comparison, we apply our matrix-free algorithm ITERGLM with residual actions to the *full* training set. We use two configurations: The first one uses recycling *without* compression (i.e. $R = \infty$), the second one uses recycling *with* compression ($R = 10$). The number of solver iterations per step is limited by $j \leq 5$.

Tracking of Performance Metrics: As performance metrics, we use accuracy, the negative log likelihood (NLL) loss and the expected calibration error (ECE) (Kumar et al., 2019) on both the training and test set. The computation of those six metrics is *not* included in the runtime reported in the results (Figure 6). First, we compute the predictive mean $m_{i,j}(\mathbf{x}_\diamond)$ and marginal variance $\text{diag}(K_{i,j}(\mathbf{x}_\diamond, \mathbf{x}_\diamond))$ (see Equations (12) and (13)) for each test input \mathbf{x}_\diamond . Then, we use the probit approximation (MacKay, 1992) to obtain the predictive probabilities

$$\boldsymbol{\pi}_\diamond = \text{softmax} \left(\frac{m_{i,j}(\mathbf{x}_\diamond)}{\sqrt{1 + \frac{\pi}{8} \text{diag}(K_{i,j}(\mathbf{x}_\diamond, \mathbf{x}_\diamond))}} \right) \in \mathbb{R}^C,$$

where the vector division is defined element-wise. This is an approximation of the integral from Section 2.3. All three performance metrics are based on the predictive probabilities.

- **Accuracy:** The prediction for \mathbf{x}_\diamond is given by $\arg \max_c([\boldsymbol{\pi}_\diamond]_c)$, i.e. by the class with the largest predictive probability. The accuracy is defined as the ratio of correctly classified data.
- **NLL Loss:** The NLL loss for \mathbf{x}_\diamond is defined as the log probability for the actual class y_\diamond , i.e. $\log([\boldsymbol{\pi}_\diamond]_{y_\diamond})$. We obtain the NLL training and test loss by averaging the individual loss values for the entire training/test set.
- **ECE:** The expected calibration error (ECE) (Kumar et al., 2019) is a measure for the calibration of the predictive probabilities. It groups the probabilities of the predicted classes (i.e. the classification confidences) into bins and, within these bins, compares the average confidence with the actual accuracy. We use `MulticlassCalibrationError` from `torchmetrics` (Detlefsen et al., 2022) with default parameter `n_bins=15`.